

Five-Degree-of-Freedom Modulation Scheme for Dual Active Bridge DC–DC Converter

Di Mou[✉], Student Member, IEEE, Quanming Luo[✉], Member, IEEE, Jia Li, Yuqi Wei[✉], Student Member, IEEE, and Pengju Sun[✉], Member, IEEE

Abstract—A five-degree-of-freedom (5-DOF) modulation scheme is proposed in this article for dual active bridge converter to improve its efficiency in a wide operation range. First, the possible operation modes of the converter under the 5-DOF is analyzed. As a result, 11 effective modes are obtained and their steady-state characteristics expressions are solved, including the inductor root-mean-square (rms) current, inductor peak-to-peak current, and transmission power, etc. It is worth mentioning that the inductor peak-to-peak current expression is simple and it can be regarded as an indicator for rms current. Thus, the peak-to-peak current is treated as the objective to obtain the optimal solutions of each mode, and the global minimum peak-to-peak (GMPP) modulation scheme is obtained. However, there are only two switches that can realize soft-switching operation in the low-power range under GMPP, which results in significant switching loss. Therefore, to further expand the soft-switching operation range in the low-power range, the soft-switching conditions are also taken into consideration, and an optimized five-degree-of-freedom (O5-DOF) modulation scheme is proposed. With the proposed O5-DOF, almost all switches can realize soft-switching operation during the whole load range, and the inductor rms current is minimized simultaneously. Finally, the experimental results are presented to validate the theoretical analysis and effectiveness of the proposed modulation scheme.

Index Terms—Dual active bridge (DAB), peak-to-peak current, root-mean-square current, soft-switching.

I. INTRODUCTION

IN RECENT years, with the rapid development of distributed renewable energy and the increasing demand of end-user with dc loads, the power supply system is evolving toward a new model of “integrated distributed photovoltaic + low voltage dc power supply + energy storage” [1]. In order to realize the interconnection between energy sources and loads, dc transformers have a high research and application value [2]. Among

Manuscript received September 21, 2020; revised December 8, 2020; accepted January 21, 2021. Date of publication February 4, 2021; date of current version June 1, 2021. Recommended for publication by Associate Editor R. Ayyanar. (*Corresponding author: Quanming Luo*)

Di Mou, Jia Li, and Pengju Sun are with the State Key Laboratory of Power Transmission Equipment, System Security and New Technology, School of Electrical Engineering, Chongqing University, Chongqing 400044, China (e-mail: dimou428@126.com; 1374702492@qq.com; spengju@cqu.edu.cn).

Quanming Luo is with the College of Electrical Engineering, Chongqing University, Chongqing 400044, China (e-mail: lqm394@126.com).

Yuqi Wei is with the Department of Electrical Engineering, University of Arkansas Fayetteville, Fayetteville, AR 72701 USA (e-mail: 1833255057@163.com).

Color versions of one or more of the figures in this article are available online at <https://doi.org/10.1109/TPEL.2021.3056800>.

Digital Object Identifier 10.1109/TPEL.2021.3056800

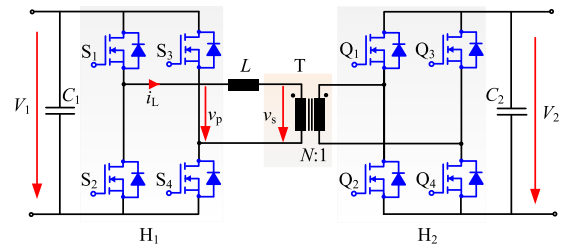


Fig. 1. Topology of DAB converter.

different dc transformer topologies, the dual active bridge (DAB) converter has gradually become the core topology due to its characteristic of symmetrical structure, large transmission power capacity, and zero voltage switching (ZVS) operation capability [3]–[5].

The topology of the DAB is shown in Fig. 1; the two H-bridges are connected through a high-frequency (HF) transformer and a power inductor, where the inductor acting as the main energy transfer device [6]. The research on the DAB is mainly focusing on the modulation schemes to improve its efficiency performance. The simplest modulation scheme for the DAB is phase-shift modulation (PSM), which only adopts one degree-of-freedom to control the direction and magnitude of power transmission [7], [8]. However, the main disadvantage of PSM is that when the voltage conversion ratio is away from unity, the soft-switching operation region becomes narrow, resulting in significant switching losses. Furthermore, there is a high reactive power under light load conditions, which leads to high conduction loss [9], [10]. Therefore, PSM is not suitable for the energy storage system and dc power supply with a wide voltage conversion range.

Currently, in order to overcome the shortcomings of PSM, numerous optimized modulation schemes have been proposed [11]–[21], [23]–[29], which can be mainly classified into the following five categories.

- 1) *Variable Inductor and Frequency Technique* [11], [12]: It attempts to change the relationship between inductor or frequency and steady-state characteristics such as current and transmission power, thereby improving the performance of the DAB converter. However, this approach makes it harder to optimize the magnetics and filter. Besides, the converter may work at a very high switching frequency under light load conditions, which degrades its electromagnetic interference (EMI) performance.

- 2) *Voltage Offset Technique* [13]: It introduces a voltage offset across the dc blocking capacitors on both sides, and the converter can switch between different operating modes to lower the inductor current according to different operating conditions. However, this approach increases the cost and degrades the converter power density.
- 3) *Dead Time Technique* [14]: It is capable of expanding the soft-switching operation region by making the dead time equal to the transient time for realizing soft switching. Because it is based on transients, the demand for sampling and computing power is very high, which will increase system cost and computational complexity.
- 4) *Burst Mode Technique* [15], [16]: It enables the converter to be in a full-load state during the working state, so that the inductor current reaches a sufficiently high value, and thus improves the efficiency of the converter under light load conditions. However, since burst mode control increases the ripple component related to the burst frequency, a large capacitor must be used at the output, which is not preferred for high power density applications.
- 5) *Phase-Shift Technique* [4], [17]–[21], [22]–[29]: It improves the steady-state characteristics by increasing the degree-of-freedom, thereby adjusting the phase-shift angle in the bridges. Compared with the other four methods, this method is easy to be implemented and only needs to be modified at the software level without modifying the hardware.

Obviously, from the perspective of cost, power density, and efficiency, the phase-shift technique is more attractive and advantageous.

For the existing phase-shift techniques, according to the number of degrees-of-freedom, it mainly includes the two-degrees-of-freedom modulation scheme and three-degrees-of-freedom modulation scheme. The extended-phase-shift (EPS) and dual-phase-shift (DPS) belong to the two-degrees-of-freedom modulation scheme [17], [18]. While the three-degrees-of-freedom scheme includes triple-phase-shift (TPS) [19]–[21], [24], [26]–[28] and asymmetric duty modulation (ADM) [25]. When compared with PSM, EPS introduces a new degree-of-freedom in one of the full bridges, while DPS introduces the same degrees-of-freedom in the two full bridges. They can effectively reduce reactive power and current stress and expand the soft-switching operation range. However, the amount of reactive power under light load operations for EPS and DPS are still large. TPS introduces two different degrees-of-freedom in the two full bridges, and the obtained HF ac voltage waveforms are symmetrical within half of a switching period and contain two zero-voltage portions within one switching period. The global optimal modulation (GOM) scheme proposed in [19] and fundamental duty modulation (FDM) scheme proposed in [20] are typical TPS. Both of them can be calculated online and are easy to be realized. Moreover, the efficiency of the converter under light load operation is significantly improved compared with other TPS. For GOM, the inductor rms current is minimized in the whole load range, and thereby, the conduction loss is reduced significantly. However, there are six switches that lose ZVS switching condition, thus leading to high switching losses. As for the FDM scheme, although

the range of soft-switching is extended, the actual inductor rms current cannot be reduced to the minimum because only the fundamental component is considered in the optimization process, which leads to significant conduction loss, especially at light load. ADM is another three-degrees-of-freedom modulation scheme. The obtained HF ac voltage waveforms under this scheme are composed of two continuous voltage pulses with opposite polarity and each switching period contains only one zero voltage portion. It extends the soft-switching operation region to some extent, but the inductor rms current becomes larger when compared with TPS. Obviously, to fully utilize the DAB converter, the three-degrees-of-freedom modulation schemes are not sufficient to improve the efficiency over the entire load range.

In this article, a five-degrees-of-freedom (5-DOF) modulation scheme is proposed by adding two new degrees-of-freedom based on TPS and ADM. For the 5-DOF modulation scheme, the high-frequency ac voltage waveform consists of two continuous voltage pulses with opposite polarity, and each switching period contains two unequal zero-voltage portion. Therefore, from the perspective of the transformer terminal voltage, it is mainly to adjust the value and position of the zero-voltage portions in the three-level waveform by increasing the degree-of-freedom. As the degree-of-freedom increases, more flexibility can be provided to minimize the rms current and maximize the soft-switching range to improve the performance of the converter. Accordingly, an optimized five-degree-of-freedom (O5-DOF) modulation scheme is proposed, which can make almost all switches realize soft-switching operation over the whole load range, and the inductor rms current is minimized at the same time. Moreover, this modulation scheme still maintains the characteristic of simplicity.

The rest of this article is organized as follows. Section II mainly introduces the typical operating waveforms and mode classification of the 5-DOF modulation scheme. In Section III, the expressions of the steady-state characteristics of each mode, including the transmission power, the inductor peak-to-peak current, and inductor rms current are derived. Then, the global minimum peak-to-peak (GMPP) current scheme is proposed in Section IV. However, the soft-switching range of this modulation method still needs to be further improved. Therefore, in Section V, the ZVS condition is added as an optimization goal, and the O5-DOF is obtained. The experimental results are presented in Section VI to validate the effectiveness of the O5-DOF modulation scheme. Finally, the conclusion is drawn in Section VII.

II. MODE CLASSIFICATION

As shown in Fig. 1, V_1 and V_2 represent the input voltage and output voltage of the DAB converter, respectively. v_p and v_s represent the transformer primary and secondary voltages, respectively, and i_L is the inductor current. In the circuit, C_1 and C_2 are the dc-side supporting capacitors, $N:1$ represents the turns ratio of the transformer, and L represents the total inductor, which is the sum of the transformer leakage and additional inductor. The inductors are used as energy storage element. The symmetrical structure enables the converter to transmit power

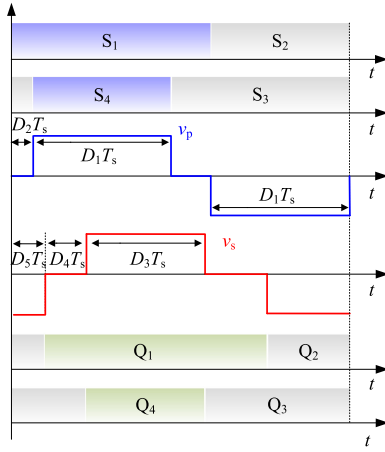


Fig. 2. Typical waveforms of the 5-DOF modulation scheme.

in both directions. According to the direction of the transmitted power P and the voltage conversion ratio $M = (NV_2/V_1)$, the converter can work in the following four different situations [12]:

- 1) forward/buck ($P > 0, M < 1$);
- 2) forward/boost ($P > 0, M > 1$);
- 3) backward/buck ($P < 0, M < 1$);
- 4) backward/boost ($P > 0, M > 1$).

Since the analysis for these four modes are similar, the forward/buck mode is sufficient to demonstrate the analyzing procedures and optimization process.

A. Operational Principles

The gate signals, transformer primary voltage v_p , and secondary voltages v_s of the 5-DOF over one switching period are shown in Fig. 2, where T_s is the switching period. For the primary side, the duration of the high and low levels of v_p is defined as $D_1 T_s$, and $D_2 T_s$ is the phase-shift between switches S_1 and S_4 . Similarly, for the secondary, the duration of the high and low levels of v_s is defined as $D_1 T_s$, and $D_4 T_s$ is the phase-shift between switches Q_1 and Q_4 . Moreover, there is another independent degree-of-freedom, that is, the phase-shift between switches S_1 and Q_1 , which is defined as $D_5 T_s$. In general, these parameters need to meet the following constraints:

$$\begin{cases} 2D_1 + D_2 \leq 1, 2D_3 + D_4 \leq 1 \\ 0 \leq D_1, D_3, D_5 \leq 0.5. \end{cases} \quad (1)$$

Therefore, by modulating D_1-D_5 , the magnitude and phase of the inductor voltage can be controlled, which in turn control the magnitude and flow of power transmission. As can be observed from Fig. 2, the most significant feature of the HF ac voltages v_p and v_s is that they contain two unequal zero-voltage portions within one switching period. Compared with TPS and ADM, 5-DOF improves control flexibility by increasing the degrees-of-freedom. It is worth noting that among these 5-DOF, when $D_1 + D_2 = 0.5$ and $D_3 + D_4 = 0.5$, it is the TPS; when $D_2 = 0$ and $D_4 = 0$, it is the ADM; when $D_1 = 0.5$, $D_2 = 0$, $D_3 + D_4 = 0.5$ or $D_3 = 0.5$, $D_4 = 0$, and $D_1 + D_2 = 0.5$, it is the EPS; when $D_1 + D_2 = 0.5$, $D_3 + D_4 = 0.5$, and $D_1 = D_3$, it is the DPS; when $D_1 = 0.5$, $D_2 = 0$, $D_3 = 0.5$, and $D_4 = 0$, it is the PSM.

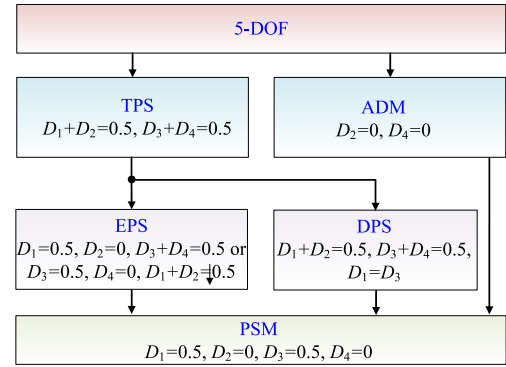


Fig. 3. Relationships among different modulation schemes.

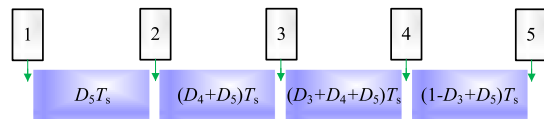


Fig. 4. Arrangement of secondary-side voltage switching time.

0, it is the traditional PSM, and their specific relationships are shown in Fig. 3. Therefore, the proposed 5-DOF can well unify these existing modulation schemes; namely, EPS, DPS, TPS, and ADM are all special cases of it.

Modeling and analysis of the DAB converter is the basis of optimization [23]. Currently, the modeling and analysis methods are adopted to obtain the steady-state characteristics of the DAB converter, which can be categorized into the time domain analysis (TDA) and frequency-domain analysis (FDA). The TDA-based method is intuitive and precise, which is widely used in the literature. Generally, for the studies under TDA, it is necessary to divide the switching period into different stages and derive the operating models. In contrast, FDA-based modeling does not need to discuss different modes; thus, the modeling process is simple. However, the steady-state characteristics obtained by this method are not conducive to obtaining accurate or direct optimization results from the fundamental and higher order forms. Therefore, the TDA method is selected in the following analysis.

B. Operating Mode Classification

As can be seen from Fig. 2, the inductor voltage may be different in a switching period, which ultimately affects the trend of i_L and forms different modes. Therefore, the operation mode of the DAB converter can be divided according to the relative positions of v_p and v_s . Specifically, it can be seen from Fig. 2 that the three-level state waveform of v_p changes at the moments of $D_2 T_s$, $(D_1 + D_2) T_s$, and $(1 - D_1) T_s$, respectively. Similarly, v_s changes at the moments of $D_5 T_s$, $(D_4 + D_5) T_s$, $(D_3 + D_4 + D_5) T_s$, and $(1 - D_3 + D_5) T_s$ in a switching period. Thus, the mode classification of the DAB converter under 5-DOF is basically determined by order of these seven switching moments. The specific classification and discussion are made as follows.

First, the moments that the state of v_s changes from small to large are sorted as $D_5 T_s$, $(D_4 + D_5) T_s$, $(D_3 + D_4 + D_5) T_s$, and $(1 - D_3 + D_5) T_s$, as shown in Fig. 4. It can be seen that

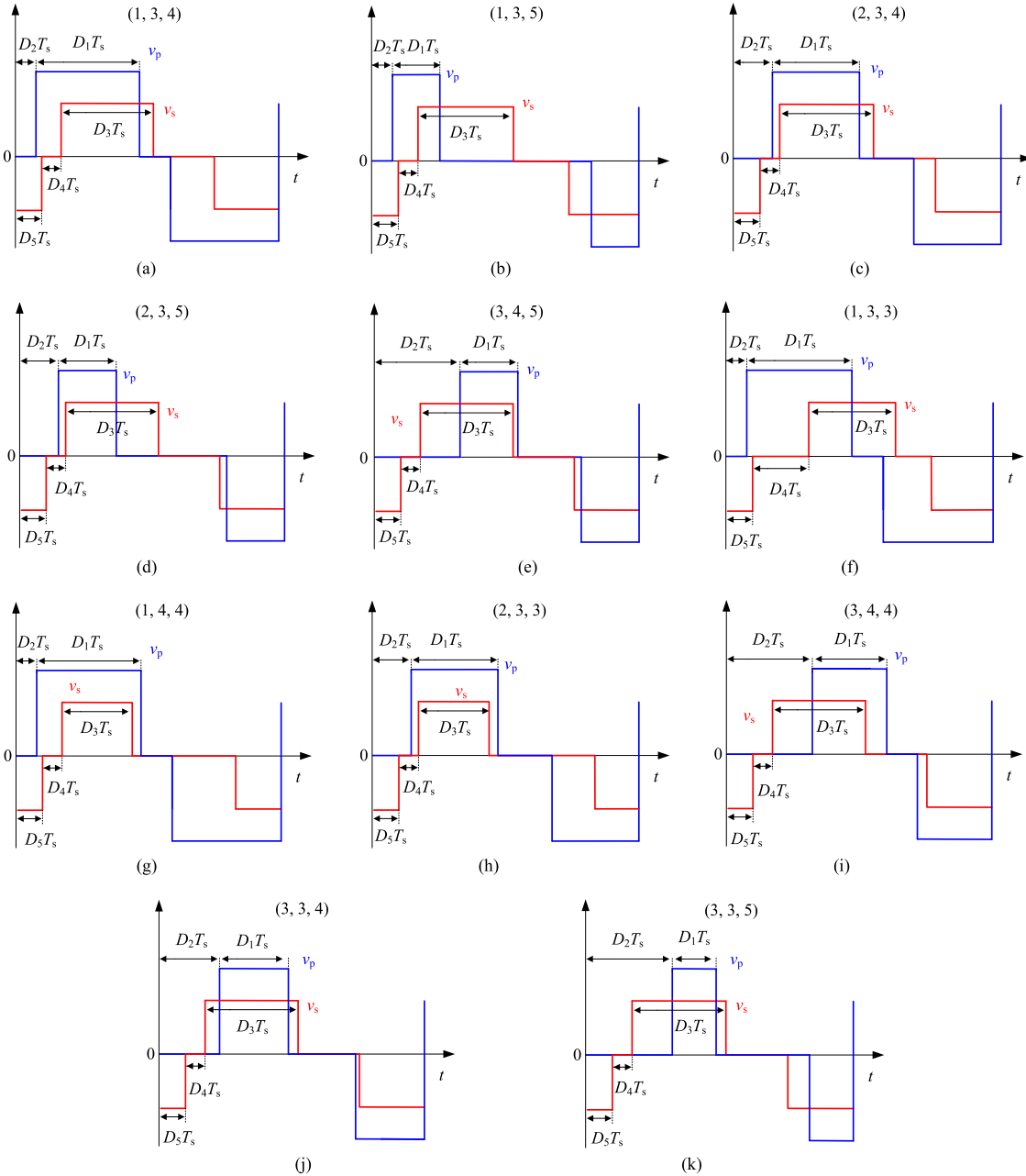


Fig. 5. Typical steady-state waveforms of the nine modulation schemes, including HF ac voltages voltage v_p , v_s . (a) Mode A. (b) Mode B. (c) Mode C. (d) Mode D. (e) Mode E. (f) Mode F. (g) Mode G. (h) Mode H. (i) Mode I. (j) Mode J. (k) Mode K.

there are five intervals between these four moments, which are represented by “1,” “2,” “3,” “4,” and “5,” respectively. Then, inserting the switching moment when the state of v_p changes into these five intervals, different modes will be derived.

- Assuming that only one switching moment of v_p can be scheduled for each interval, it will form $C_5^3 = 10$ combinations. For example, when $D_2 T_s$, $(D_1 + D_2) T_s$ and $(1 - D_1) T_s$ are inserted into the intervals “1,” “2,” and “3,” respectively, a combination $(1, 2, 3)$ will be formed. In these combinations, when $(D_1 + D_2) T_s$ is smaller than $(D_4 + D_5) T_s$, there is a sizeable reactive power [12], so this type of combination is not considered in this article, including $(1, 2, 3)$, $(1, 2, 4)$, and $(1, 2, 5)$. Moreover, it is

impossible to satisfy simultaneously $(D_3 + D_4 + D_5) T_s < (D_1 + D_2) T_s$ and $(1 - D_3 + D_5) T_s < (1 - D_1) T_s$ in the combination $(1, 4, 5)$ and $(2, 4, 5)$. Therefore, there are five modes left, including $(1, 3, 4)$, $(1, 3, 5)$, $(1, 4, 5)$, $(2, 3, 4)$, $(2, 3, 5)$, and $(3, 4, 5)$, which correspond to the modes A to E shown in Fig. 5, respectively.

- Assuming that the two switching moments of v_p are tied together to insert into the same intervals. Therefore, there will be two situations. One is that $D_2 T_s$ and $(D_1 + D_2) T_s$ are tied together, and the other is that $(D_1 + D_2) T_s$ and $(1 - D_1) T_s$ are tied together. As mentioned above, when $(D_1 + D_2) T_s$ is smaller than $(D_4 + D_5) T_s$, there is considerable reactive power. Besides, for the same reason,

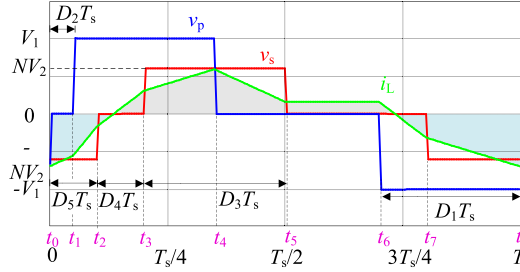


Fig. 6. General waveforms of v_p , v_s and i_L for DAB converter under mode A.

$D_2 T_s$ must be less than $(D_3 + D_4 + D_5) T_s$, $(D_1 + D_2) T_s$ must be less than $(1 - D_3 + D_5) T_s$, $(D_3 + D_4 + D_5) T_s$ must be less than $(1 - D_1) T_s$. Therefore, when $D_2 T_s$ and $(D_1 + D_2) T_s$ are tied together to meet the above requirements, there are four combinations (1, 4, 4), (2, 3, 3), (2, 4, 4), and (3, 4, 4) corresponding to modes F to I respectively, as shown in Fig. 5. Besides, when $D_2 T_s$ and $(D_1 + D_2) T_s$ are tied together, it can only be inserted into interval “3,” then the remaining $(1 - D_1) T_s$ can be inserted into “4” and “5.” Thus, two modes are formed, corresponding to modes F and G, respectively.

- 3) Assuming that three switching moments of v_p are tied together. Obviously, there is no effective mode. Depending on these seven changing moments of v_p and v_s , 11 possible modes are derived. For different operating modes, the corresponding transmission power calculation formula and the switching current expression of each switching device are different. Therefore, in the next section, the steady-state characteristics of each mode will be derived.

III. STEADY-STATE ANALYSIS

Since there are many modes, mode A is chosen as an example to demonstrate the calculation and analysis in this section, and the following assumptions are made.

- 1) The converter is operating in steady-state.
- 2) All switches are ideal.
- 3) The transformer is an ideal one with the infinite magnetizing inductor.

The waveforms are shown in Fig. 6 for mode A. In the following, the piece-wise linearity method will be used to solve the

inductor current of each interval. For the sake of analysis, all the parameters are reflected to the primary side of the transformer. Accordingly, with the 5-DOF modulation scheme, the inductor current $i_L(t)$ can be expressed as follows:

$$i_L(t) = \begin{cases} i_L(t_0) + \frac{NV_2}{L}(t - t_0) & t_0 \leq t \leq t_1 \\ i_L(t_1) + \frac{V_1 + NV_2}{L}(t - t_1) & t_1 \leq t \leq t_2 \\ i_L(t_2) + \frac{V_1}{L}(t - t_2) & t_2 \leq t \leq t_3 \\ i_L(t_3) + \frac{V_1 - NV_2}{L}(t - t_3) & t_3 \leq t \leq t_4 \\ i_L(t_4) - \frac{NV_2}{L}(t - t_4) & t_4 \leq t \leq t_5 \\ i_L(t_6) - \frac{V_1}{L}(t - t_6) & t_6 \leq t \leq t_7 \\ i_L(t_7) + \frac{NV_2 - V_1}{L}(t - t_7) & t_7 \leq t \leq T_s. \end{cases} \quad (2)$$

It can be seen from Fig. 6 that there are some relationships between periods and degrees-of-freedom, which can be summarized as follows: $t_1 - t_0 = D_2 T_s$, $t_2 - t_1 = (D_5 - D_2) T_s$, $t_3 - t_2 = D_4 T_s$, $t_4 - t_3 = (D_1 + D_2 - D_4 - D_5) T_s$, $t_5 - t_4 = (D_3 + D_4 + D_5 - D_1 - D_2) T_s$, $t_6 - t_5 = (1 - D_1 - D_3 - D_4 - D_5) T_s$, and $t_7 - t_6 = (D_1 + D_5 - D_3) T_s$. Substituting them into (2), the inductor current values at the switching instants can be deduced as follows:

$$\left\{ \begin{array}{l} i_L(t_5) = \frac{D_1^2 V_1 + D_1 D_2 V_1 - D_3^2 N V_2 - D_3 D_4 N V_2}{f_s L} \\ i_L(t_0) = i_L(t_5) - \frac{D_1 V_1 - D_3 N V_2 + D_5 N V_2}{f_s L} \\ i_L(t_1) = i_L(t_5) - \frac{D_1 V_1 - D_2 N V_2 - D_3 N V_2 + D_5 N V_2}{f_s L} \\ i_L(t_2) = i_L(t_5) - \frac{D_1 V_1 + D_2 V_1 - D_5 V_1 - D_3 N V_2}{f_s L} \\ i_L(t_3) = i_L(t_5) + \frac{D_4 V_1 - D_2 V_1 - D_1 V_1 + D_5 V_1 + D_3 N V_2}{f_s L} \\ i_L(t_4) = i_L(t_5) + \frac{(D_3 - D_2 - D_1 + D_4 + D_5) N V_2}{f_s L} \\ i_L(t_7) = i_L(t_5) - \frac{V_1 (D_1 - D_3 + D_5)}{f_s L}. \end{array} \right. \quad (3)$$

From (3), the inductor rms current can be derived as (4) shown at the bottom of this page. It can be seen that the inductor rms current has a very complex expression, and strong coupling between different degrees-of-freedom exists. Obviously, if rms current is chosen as the optimization objective, it is difficult to get a simple analytical solution

$$I_{\text{rms}} = \sqrt{\frac{1}{T_s} \int_0^{T_s} i(t)^2 dt} = \sqrt{\frac{V_1^2 (-3D_1^4 - 6D_1^3 D_2 + 2D_1^3 - 3D_1^2 D_2^2 + 3D_1^2 D_2)}{3(f_s L)^2} + N V_1 V_2 \left(\begin{array}{l} D_1^3 + 6D_1^2 D_3^2 + 6D_1^2 D_3 D_4 - 3D_1^2 D_3 - D_4^3 \\ -3D_1^2 D_5 + 3D_1 D_2^2 + 6D_1 D_2 D_3^2 + 3D_3 D_5^2 \\ -6D_1 D_2 D_3 - 6D_1 D_2 D_4 - 6D_1 D_2 D_5 + D_3^3 \\ +6D_1 D_3 D_5 + 3D_1 D_4^2 + 6D_1 D_4 D_5 + 3D_1 D_5^2 \\ +2D_2^3 - 3D_2^2 D_4 - 6D_2^2 D_5 + 3D_2 D_4^2 - 3D_5^3 \\ +6D_1 D_2 D_3 D_4 + 6D_2 D_5^2 - 3D_1 D_3^2 + 3D_3 D_5^2 \\ -3D_4^2 D_5 - 3D_4^2 D_5^2 + 6D_2 D_4 D_5 - 3D_1 D_4^2 \end{array} \right) + N^2 V_2^2 (-3D_3^4 - 6D_3^3 D_4 + 2D_3^3 - 3D_3^2 D_4 - 3D_3^2 D_5)}{3(f_s L)^2} } \quad (4)$$

Therefore, a more straightforward optimization objective is needed. In this mode, the current is rising from t_0 to t_4 , and falling from t_4 to t_8 . Accordingly, the maximum value of the current appears at the moment t_4 , and the minimum value of the current appears at the moment t_0 . Thus, the inductor peak-to-peak current can be obtained as follows:

$$I_{\text{p-p}} = \frac{D_1 V_1 - D_1 N V_2 - D_2 N V_2 + D_4 N V_2 + 2 D_5 N V_2}{f_s L} \quad (5)$$

It can be seen from (5) that the expression of inductor peak-to-peak current $I_{\text{p-p}}$ is very simple, and it can be regarded as a symbol of rms current under the same output power. Then, the average output power can be calculated as follows:

$$\begin{aligned} P &= \frac{1}{T_s} \int_0^{T_s} v_p i_L dt \\ &= \frac{N V_1 V_2}{f_s L} \left(\begin{array}{l} D_1^2 + 2 D_1 D_2 - 2 D_1 D_3 - 2 D_1 D_4 \\ - 2 D_1 D_5 + 2 D_2^2 - 2 D_2 D_4 - 4 D_2 D_5 \\ + D_3^2 - 2 D_3 D_5 + D_4^2 + 2 D_4 D_5 + 3 D_5^2 \end{array} \right). \end{aligned} \quad (6)$$

In order to simplify the analysis and calculation of $I_{\text{p-p}}$ and P , they are normalized as follows:

$$\begin{cases} P' = \frac{P}{P_b} = 2\pi M \\ \left(\begin{array}{l} D_1^2 + 2 D_1 D_2 - 2 D_1 D_3 - 2 D_1 D_4 \\ - 2 D_1 D_5 + 2 D_2^2 - 2 D_2 D_4 - 4 D_2 D_5 \\ + D_3^2 - 2 D_3 D_5 + D_4^2 + 2 D_4 D_5 + 3 D_5^2 \end{array} \right) \\ I'_{\text{p-p}} = \frac{I_{\text{p-p}}}{I_b} = 2\pi (D_1 - D_1 M + 2 D_3 M) \end{cases} \quad (7)$$

where I_b and P_b are defined as follows:

$$\begin{cases} I_b = \frac{V_1}{2\pi f_s L} \\ P_b = \frac{V_1^2}{2\pi f_s L} \end{cases} \quad (8)$$

Thus, the steady-state characteristics of mode A are derived completely, including transmission power, inductor rms current, inductor peak-to-peak current, etc. Similarly, the unified expressions of inductor peak-to-peak current and transmission power for other modes can be summarized, and are shown in Table I. Due to the complexity of rms current, it is not included in Table I. Combined with the constraints among degrees-of-freedom, the transmission power range of each mode is shown in Fig. 7. It can be found from Fig. 7 that only mode F can cover the entire load range. For modes I and K, the transmission power range is the narrowest and can only reach $\pi M/8$. Besides, for mode E, the transmission power is negative, which is not shown.

It can be seen from Table I that the expressions of inductor peak-to-peak current obtained by modes G, H, and J are different from other modes. The reason lies in that these modes are different from the value of $D_1 + D_2$ and $D_3 + D_4 + D_5$. Specifically, modes G, H, and J satisfy the relationship $D_1 +$

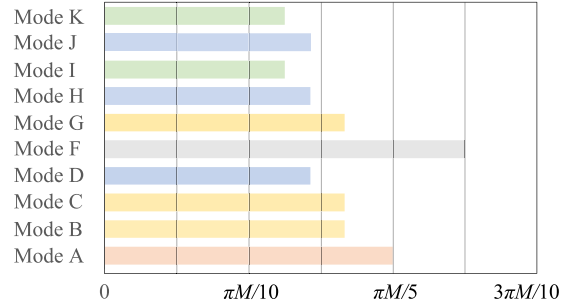


Fig. 7. Ranges of transmission power for different modes.

$D_2 > D_3 + D_4 + D_5$, while the others satisfy $D_1 + D_2 < D_3 + D_4 + D_5$. Thus, for these three modes, the following relationship is always satisfied:

$$\begin{aligned} 2\pi (D_1 - D_3 M + D_5 M) &< I'_{\text{pp}} \\ &= 2\pi \left[D_1 - M \left(\begin{array}{c} D_1 + D_2 \\ - D_4 - 2 D_5 \end{array} \right) \right]. \end{aligned} \quad (9)$$

It can be seen from (9) that the inductor peak-to-peak currents of modes G, H, and J are always larger than those of other modes when the degrees-of-freedom are given. Therefore, these three modes G, H, and J are not analyzed here since they do not have advantages in terms of peak-to-peak current. According to the analysis above, when the parameters of the circuit are determined, there are multiple combinations of D for specific transmission power, so the circuit operation can be improved by selecting appropriate D under the premise of satisfying the transmission power. In the next section, the optimal path will be presented.

IV. GLOBAL MINIMUM PEAK-TO-PEAK CURRENT SCHEME

For the DAB converter, losses are generally divided into switching losses, conduction losses, and magnetic losses [20]. Generally, the optimization targets are usually set as switching losses or conduction losses since the core loss will not change obviously. In this article, because there are many possible modes, considering these two goals at the same time will make the optimization process very complicated. In order to simplify the calculation, in this section, the conduction loss is first chosen as the optimization objective. The optimization of conduction loss can be converted into the optimization of rms current because conduction loss is proportional to rms current. However, as can be seen from (4), the rms current itself requires intensive calculations. As mentioned above, a simple and effective method is to select the peak-to-peak current of the inductor as the optimization objective, which can be used as an indicator for rms current.

TABLE I
OUTPUT POWER AND PEAK-TO-PEAK EXPRESSIONS

Mode operational constraints		Transmission power	Peak-to-peak inductor current
A	$\begin{cases} D_2 \leq D_5, D_5 + D_4 \leq D_1 + D_2 \\ D_1 + D_2 \leq D_3 + D_4 + D_5, D_3 \leq D_1 + D_5 \\ D_3 + D_4 + D_5 \leq 1 - D_1 \end{cases}$	$P' = -\pi M \left(\begin{array}{l} D_1^2 + 2D_1 D_2 - 2D_1 D_3 - 2D_1 D_4 - 2D_1 D_5 + 2D_2^2 - 2D_2 D_4 \\ -4D_2 D_5 + D_3^2 - 2D_3 D_5 + D_4^2 + 2D_4 D_5 + 3D_5^2 \end{array} \right)$	
B	$\begin{cases} D_2 \leq D_5, D_5 + D_4 \leq D_1 + D_2 \\ D_1 + D_2 \leq D_3 + D_4 + D_5 \\ 2D_3 + D_4 \leq 1, D_1 + D_5 \leq D_3 \end{cases}$	$P' = -\pi M \left(\begin{array}{l} 2D_2^2 - 2D_2 D_4 - 4D_2 D_5 + 2D_1 D_2 + D_4^2 \\ + 2D_4 D_5 - 2D_1 D_4 + 2D_3^2 - 4D_1 D_5 \end{array} \right)$	
C	$\begin{cases} D_5 \leq D_2, D_1 + D_2 \leq D_3 + D_5 + D_4 \\ D_5 + D_4 \leq D_1 + D_2, D_2 \leq D_3 + D_4 \\ D_3 + D_5 + D_4 \leq 1 - D_1, D_3 \leq D_1 + D_5 \end{cases}$	$P' = -\pi M \left(\begin{array}{l} D_1^2 + 2D_1 D_2 - 2D_1 D_3 - 2D_1 D_4 - 2D_1 D_5 + D_2^2 - 2D_2 D_4 \\ -2D_2 D_5 + D_3^2 - 2D_3 D_5 + D_4^2 + 2D_4 D_5 + 2D_5^2 \end{array} \right)$	$I'_{pp} = 2\pi \left[D_1 - M \left(\begin{array}{l} D_1 + D_2 \\ -D_4 - 2D_5 \end{array} \right) \right]$
D	$\begin{cases} D_5 \leq D_2, D_1 + D_2 \leq D_3 + D_5 + D_4 \\ D_5 + D_4 \leq D_1 + D_2, D_2 \leq D_3 + D_4 \\ 2D_3 + D_4 \leq 1, D_5 + D_1 \leq D_3 \end{cases}$	$P' = -\pi M \left(\begin{array}{l} D_2^2 - 2D_2 D_4 - 2D_2 D_5 + 2D_1 D_2 + D_4^2 \\ + 2D_4 D_5 - 2D_1 D_4 + D_5^2 - 4D_1 D_5 \end{array} \right)$	
E	$\begin{cases} D_5 \leq D_2, D_1 + D_2 \leq D_3 + D_5 + D_4 \\ D_5 + D_4 \leq D_1 + D_2, D_2 \leq D_3 + D_4 \\ D_3 + D_5 + D_4 \leq 1 - D_1, D_3 \leq D_1 + D_5 \end{cases}$	$P' = -\pi M \left(\begin{array}{l} D_1^2 + 2D_1 D_2 - 2D_1 D_3 - 2D_1 D_4 - 2D_1 D_5 + D_2^2 - 2D_2 D_4 \\ -2D_2 D_5 + D_3^2 - 2D_3 D_5 + D_4^2 + 2D_4 D_5 + 2D_5^2 \end{array} \right)$	
F	$\begin{cases} D_2 \leq D_5, D_5 + D_4 \leq D_1 + D_2 \\ 2D_1 + D_2 \leq 1, 2D_3 + D_4 \leq 1 \\ 1 - D_1 \leq D_3 + D_4 + D_5 \end{cases}$	$P' = -\pi M \left(\begin{array}{l} 2D_1^2 + 2D_1 D_2 - 2D_1 + 2D_2^2 - 2D_2 D_4 - 4D_2 D_5 + 2D_3^2 \\ + 2D_3 D_4 - 2D_3 + 2D_4^2 + 4D_4 D_5 - 2D_4 + 4D_5^2 - 2D_5 + 1 \end{array} \right)$	
G	$\begin{cases} D_2 \leq D_5, D_3 + D_4 + D_5 \leq D_1 + D_2 \\ 2D_1 + D_2 \leq 1, D_3 \leq D_1 + D_5 \end{cases}$	$P' = -\pi M \left(D_2^2 - 2D_2 D_5 + 2D_2 D_3 + 2D_5^2 - 4D_3 D_5 - 2D_3 D_4 \right)$	
H	$\begin{cases} D_5 \leq D_2, D_2 \leq D_4 + D_5 \\ D_3 + D_4 + D_5 \leq D_1 + D_2 \\ D_3 \leq D_1 + D_5 \end{cases}$	$P' = -\pi M \left(D_5^2 - 4D_3 D_5 + 2D_2 D_3 - 2D_3 D_4 \right)$	$I'_{pp} = 2\pi (D_1 - D_3 M + D_5 M)$
I	$\begin{cases} D_5 + D_4 \leq D_2, D_2 \leq D_3 + D_4 + D_5 \\ D_3 + D_4 + D_5 \leq D_1 + D_2, D_3 \leq D_1 + D_5 \end{cases}$	$P' = \pi M (2D_3 - D_2 + D_4)(D_4 - D_2 + 2D_5)$	
J	$\begin{cases} D_1 + D_2 \leq D_3 + D_4 + D_5 \\ D_3 + D_4 + D_5 \leq 1 - D_1 \\ D_3 \leq D_1 + D_2 \end{cases}$	$P' = -\pi M \left(D_1^2 + D_3^2 + D_5^2 + 2D_1 D_2 - 2D_1 D_3 - 2D_1 D_4 - 2D_1 D_5 - 2D_3 D_5 \right)$	$I'_{pp} = 2\pi \left[D_1 - M \left(\begin{array}{l} D_1 + D_2 \\ -D_4 - 2D_5 \end{array} \right) \right]$
K	$\begin{cases} D_5 + D_4 \leq D_2, D_1 + D_2 \leq D_3 + D_4 + D_5 \\ D_1 + D_5 \leq D_3 \end{cases}$	$P' = 2\pi D_1 M (D_4 - D_2 + 2D_5)$	

A. Optimization Method

From the above analysis, the objective function to optimize the inductor peak-to-peak current can be expressed as follows:

$$\begin{aligned} & \text{Minimize } I_{p-p}(\mathbf{D}) \\ & \text{Subject to } P'(\mathbf{D}) - P_*' \leq 0 \\ & h_i(\mathbf{D}) = 0 \quad (i = 1, 2, \dots, n) \end{aligned} \quad (10)$$

where P_*' is a unit value of specified power level and $h_i(\mathbf{D})$ is composed of the mutual constraints between the degrees-of-freedom of each mode.

Karush–Kuhn–Tucker (KKT) condition is the most suitable condition for the optimization of such problems because it is the necessary condition for the optimal solution. It can eliminate many nonoptimal solutions in the available range. Next, each mode can be solved with KKT conditions. KKT function L incorporating all constraints can be written as follows:

$$L = I'_{p-p}(\mathbf{D}) + \lambda \cdot P'(\mathbf{D}) + \sum_{i=1}^m u_i \cdot h_i(x). \quad (11)$$

In (11), λ is the Lagrange multiplier corresponding to the inequality constraint $P'(\mathbf{D})$ and μ_i is the Lagrange multiplier of equality constraint $h_i(x)$. Then, the KKT conditions are expressed as follows:

$$\begin{cases} \frac{\partial I'_{p-p}}{\partial D_j} + \lambda \frac{\partial P'}{\partial D_j} + \sum_{i=1}^n \mu_j \frac{\partial h_j}{\partial D_j} = 0 \quad (j = 1, 2, 3, 4, 5) \\ h_i(\mathbf{D}) = 0 \quad u_i g_i(\mathbf{D}) = 0 \quad u_i \geq 0 \quad \lambda \neq 0. \end{cases} \quad (12)$$

By substituting the expressions of inductor peak-to-peak current and transmission power of different modes in Table I into (10)–(12), the optimal solution of each mode can be obtained, as shown in Table II.

B. Optimization Results

Basically, it can be seen from Table II that each mode is divided into two sections within its own power range. Combined with these mode optimization solutions, the whole power range

TABLE II
OPTIMIZED SOLUTIONS FOR DIFFERENT MODES

	Power Range	Optimal solution	Power Range	Optimal solution
A	$P' \in \left(0, \frac{M^2\pi(1-M)}{2}\right]$	$\begin{cases} D_{1,\text{opt}} = \frac{D_{2,\text{opt}}M}{(1-M)}, D_{4,\text{opt}} = 0 \\ D_{3,\text{opt}} = \frac{D_{2,\text{opt}}}{(1-M)}, D_{5,\text{opt}} = D_{2,\text{opt}} \\ D_{2,\text{opt}} = \frac{\sqrt{2}P'\sqrt{(1-M)}}{2M\sqrt{\pi}} \end{cases}$	$P' \in \left(\frac{M\pi(M^2-M)}{2}, \frac{M\pi}{5}\right]$	$\begin{cases} D_{2,\text{opt}} = \frac{\sqrt{2}(5P'-\pi M)(M-1)\sqrt{\frac{5M^2-5M+2}{M(5P'-\pi M)}}}{2\sqrt{\pi}(5M^2-5M+2)} \\ D_{3,\text{opt}} = \frac{2}{5} - \frac{D_{2,\text{opt}}}{5(M-1)}, D_{4,\text{opt}} = 0 \\ D_{1,\text{opt}} = \frac{D_{2,\text{opt}}(20P'+5\pi M^2-25MP'-4\pi M)}{5(M-1)(5P'-\pi M)} + \frac{2}{5} \\ D_{5,\text{opt}} = \frac{1}{5} - \frac{D_{2,\text{opt}}(15P'+5\pi M^2-25MP'-3\pi M)}{5(M-1)(5P'-\pi M)} \end{cases}$
B	$P' \in \left(0, \frac{M^2\pi(1-M)}{2}\right]$	$\begin{cases} D_{1,\text{opt}} = \frac{D_{2,\text{opt}}M}{(1-M)}, D_{4,\text{opt}} = 0 \\ D_{3,\text{opt}} = \frac{D_{2,\text{opt}}}{(1-M)}, D_{5,\text{opt}} = D_{2,\text{opt}} \\ D_{2,\text{opt}} = \frac{\sqrt{2}P'\sqrt{(1-M)}}{2M\sqrt{\pi}} \end{cases}$	$P' \in \left(\frac{M\pi(M^2-M)}{2}, \frac{M\pi}{6}\right]$	$\begin{cases} D_{2,\text{opt}} = \frac{(6P'-\pi M)(M-1)\sqrt{\frac{3M^2-3M+1}{M(6P'-\pi M)}}}{2\sqrt{\pi}(3M^2-3M+1)} \\ D_{3,\text{opt}} = 0.5, D_{4,\text{opt}} = 0, D_{1,\text{opt}} + D_{5,\text{opt}} = 0.5 \\ D_{1,\text{opt}} = \frac{\sqrt{\frac{3M^2-3M+1}{M(6P'-\pi M)}}(12P'+3\pi M^2-18MP'-2\pi M)}{6\sqrt{\pi}(3M^2-3M+1)} + \frac{1}{3} \end{cases}$
C	$P' \in \left(0, \frac{M^2\pi(1-M)}{2}\right]$	$\begin{cases} D_{1,\text{opt}} = \frac{D_{2,\text{opt}}M}{(1-M)}, D_{4,\text{opt}} = 0 \\ D_{3,\text{opt}} = \frac{D_{2,\text{opt}}}{(1-M)}, D_{5,\text{opt}} = D_{2,\text{opt}} \\ D_{2,\text{opt}} = \frac{\sqrt{2}P'\sqrt{(1-M)}}{2M\sqrt{\pi}} \end{cases}$	$P' \in \left(\frac{M\pi(M^2-M)}{2}, \frac{M\pi}{6}\right]$	$\begin{cases} D_{2,\text{opt}} = \frac{1}{6} - \frac{\sqrt{\frac{-3M^2-3M+1}{M(6P'-\pi M)}}(12P'+3\pi M^2-18MP'-2\pi M)}{6\sqrt{\pi}(3M^2-3M+1)} \\ D_{2,\text{opt}} = D_{5,\text{opt}}, D_{4,\text{opt}} + D_{3,\text{opt}} = 0.5, D_{1,\text{opt}} + D_{5,\text{opt}} = 0.5 \\ D_{4,\text{opt}} = \frac{(6P'-\pi M)\sqrt{\frac{3M^2-3M+1}{M(6P'-\pi M)}}}{6\sqrt{\pi}(3M^2-3M+1)} + \frac{1}{6} \end{cases}$
D	$P' \in \left(0, \frac{M^2\pi(1-M)}{2}\right]$	$\begin{cases} D_{1,\text{opt}} = \frac{D_{2,\text{opt}}M}{(1-M)}, D_{4,\text{opt}} = 0 \\ D_{3,\text{opt}} = \frac{D_{2,\text{opt}}}{(1-M)}, D_{5,\text{opt}} = D_{2,\text{opt}} \\ D_{2,\text{opt}} = \frac{\sqrt{2}P'\sqrt{(1-M)}}{2M\sqrt{\pi}} \end{cases}$	$P' \in \left(\frac{M\pi(M^2-M)}{2}, \frac{M\pi}{7}\right]$	$\begin{cases} D_{1,\text{opt}} = \frac{2}{7} + \frac{\sqrt{2}\sqrt{\frac{7M^2-7M+2}{M(7P'-\pi M)}}(28P'+7\pi M^2-49MP'-4\pi M)}{14\sqrt{\pi}(7M^2-7M+2)} \\ D_{2,\text{opt}} = D_{5,\text{opt}}, D_{1,\text{opt}} + D_{2,\text{opt}} = D_{3,\text{opt}} \\ D_{2,\text{opt}} = \frac{1}{7} - \frac{\sqrt{2}\sqrt{\frac{7M^2-7M+2}{M(7P'-\pi M)}}(35P'+7\pi M^2-49MP'-5\pi M)}{14\sqrt{\pi}(7M^2-7M+2)} \\ D_{4,\text{opt}} = \frac{1}{7} + \frac{\sqrt{2}(7P'-\pi M)\sqrt{\frac{7M^2-7M+2}{M(7P'-\pi M)}}}{7\sqrt{\pi}(7M^2-7M+2)} \end{cases}$
F	$P' \in \left(0, \frac{M^2\pi(1-M)}{2}\right]$	$\begin{cases} D_{2,\text{opt}} + D_{1,\text{opt}} = \frac{1}{2}, D_{3,\text{opt}} = \frac{1}{2}, D_{4,\text{opt}} = 0 \\ D_{5,\text{opt}} = D_{2,\text{opt}}, D_{1,\text{opt}} = \frac{1}{4} - \frac{\sqrt{(8P'-\pi M)}}{4\sqrt{\pi}} \end{cases}$	$P' \in \left(\frac{M\pi(M^2-M)}{2}, \frac{M\pi}{4}\right]$	$\begin{cases} D_{2,\text{opt}} = \frac{(4P'-\pi M)(M-1)\sqrt{\frac{2M^2-2M+1}{M(4P'-\pi M)}}}{2\sqrt{\pi}(2M^2-2M+1)} \\ D_{2,\text{opt}} + D_{1,\text{opt}} = 0.5, D_{3,\text{opt}} = 0.5, D_{4,\text{opt}} = 0 \\ D_{5,\text{opt}} = \frac{1}{4} - \frac{\sqrt{\frac{2M^2-2M+1}{M(4P'-\pi M)}}(4P'+2\pi M^2-8MP'-\pi M)}{4\sqrt{\pi}(2M^2-2M+1)} \end{cases}$
J	$P' \in \left(0, \frac{M^2\pi(1-M)}{2}\right]$	$\begin{cases} D_{1,\text{opt}} = \frac{D_{2,\text{opt}}M}{(1-M)}, D_{4,\text{opt}} = 0 \\ D_{3,\text{opt}} = \frac{D_{2,\text{opt}}}{(1-M)}, D_{5,\text{opt}} = D_{2,\text{opt}} \\ D_{2,\text{opt}} = \frac{\sqrt{2}P'\sqrt{(1-M)}}{2M\sqrt{\pi}} \end{cases}$	$P' \in \left(\frac{M\pi(M^2-M)}{2}, \frac{M\pi}{7}\right]$	$\begin{cases} D_{2,\text{opt}} = \frac{2}{7} - \frac{\sqrt{2}\sqrt{\frac{7M^2-7M+2}{M(7P'-\pi M)}}(21P'+7\pi M^2-49MP'-3\pi M)}{14\sqrt{\pi}(7M^2-7M+2)} \\ D_{1,\text{opt}} = \frac{\sqrt{2}\sqrt{\frac{7M^2-7M+2}{M(7P'-\pi M)}}(28P'+7\pi M^2-49MP'-4\pi M)}{14\sqrt{\pi}(7M^2-7M+2)} + \frac{2}{7} \\ D_{3,\text{opt}} = \frac{3}{7} - \frac{\sqrt{2}(7P'-\pi M)\sqrt{\frac{7M^2-7M+2}{M(7P'-\pi M)}}}{14\sqrt{\pi}(7M^2-7M+2)} \\ D_{5,\text{opt}} = D_{2,\text{opt}}, D_{4,\text{opt}} = 0 \end{cases}$
K	$P' \in \left(0, \frac{M^2\pi(1-M)}{2}\right]$	$\begin{cases} D_{1,\text{opt}} = \frac{D_{2,\text{opt}}M}{(1-M)}, D_{4,\text{opt}} = 0 \\ D_{3,\text{opt}} = \frac{D_{2,\text{opt}}}{(1-M)}, D_{5,\text{opt}} = D_{2,\text{opt}} \\ D_{2,\text{opt}} = \frac{\sqrt{2}P'\sqrt{(1-M)}}{2M\sqrt{\pi}} \end{cases}$	$P' \in \left(\frac{M\pi(M^2-M)}{2}, \frac{M\pi}{8}\right]$	$\begin{cases} D_{1,\text{opt}} = \frac{1}{4} - \frac{(8P'-\pi M)\sqrt{\frac{1}{M(8P'-\pi M)}}}{4\sqrt{\pi}} \\ D_{3,\text{opt}} = \frac{1}{2}, D_{5,\text{opt}} = D_{2,\text{opt}}, D_{4,\text{opt}} = 0 \\ D_{2,\text{opt}} = \frac{(8P'-\pi M)\sqrt{\frac{1}{M(8P'-\pi M)}}}{4\sqrt{\pi}} + \frac{1}{4} \end{cases}$

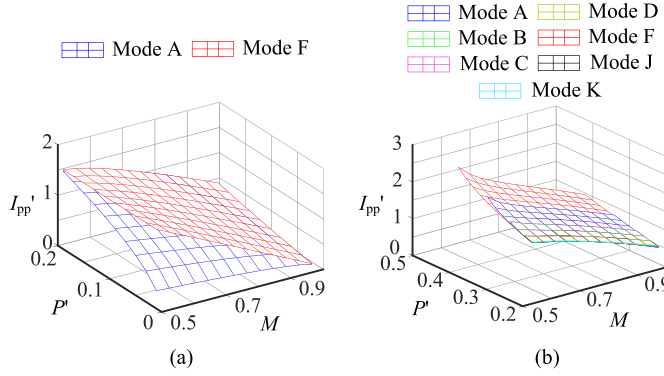


Fig. 8. Comparison of each power segment.

of $(0, \pi M/4)$ is divided into the following six segments according to the optimized solutions of each mode:

- 1) $P' \in (0, \pi M^2(1 - M)/2]$;
- 2) $P' \in (\pi M^2(1 - M)/2, \pi M/8]$;
- 3) $P' \in (\pi M/8, \pi M/7]$;
- 4) $P' \in (\pi M/7, \pi M/6]$;
- 5) $P' \in (\pi M/6, \pi M/5]$;
- 6) $P' \in (\pi M/5, \pi M/4]$.

In order to get the optimal solution for each power section, we need to compare the optimal results of different modes for each power section. The method used here is to bring the optimal solution of each degree-of-freedom obtained in Table II into (7) to solve the specific inductor peak-to-peak current of each mode under different working conditions. As a result, the peak-to-peak current comparison results of each mode are shown in Fig. 8.

In the power section $(0, \pi M^2(1 - M)/2]$, the optimized solution obtained by modes A to D and modes J to K are the same, and they have absolute advantages over mode F, as shown in Fig. 8(a). In the power section $(\pi M^2(1 - M)/2, \pi M/4]$, the inductor peak-to-peak current obtained by mode K has the minimum value, as shown in Fig. 8(b). In summary, the whole power section is divided into two parts, and the optimal solution of the low-power segment is as follows:

$$\begin{cases} D_{1,\text{opt}} = \frac{D_{2,\text{opt}} M}{(1 - M)}, D_{4,\text{opt}} = 0, D_{3,\text{opt}} = \frac{D_{2,\text{opt}}}{(1 - M)} \\ D_{5,\text{opt}} = D_{2,\text{opt}}, D_{2,\text{opt}} = \frac{\sqrt{2} P' \sqrt{\frac{(1-M)}{P'}}}{2M\sqrt{\pi}}. \end{cases} \quad (13)$$

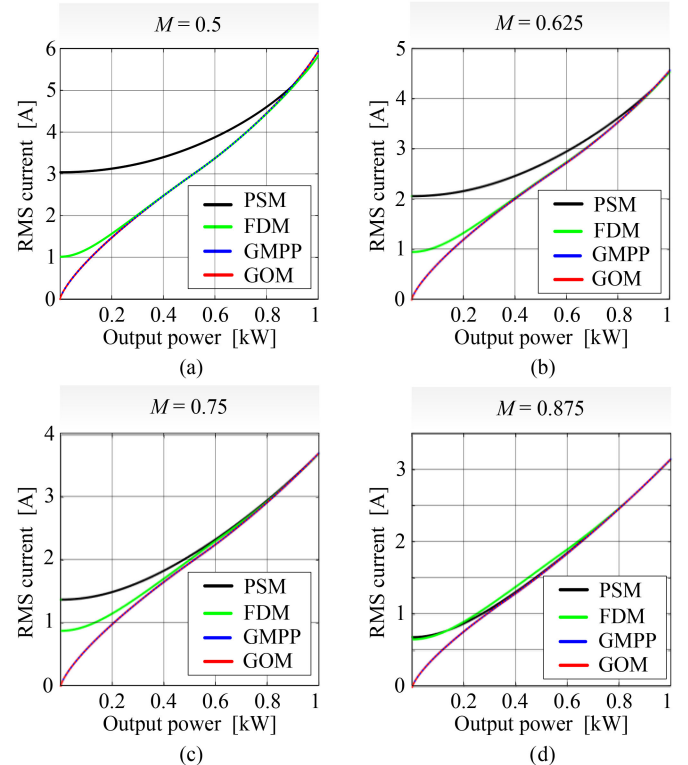
For the high-power segment, the optimal solution is as follows:

$$\begin{cases} D_{2,\text{opt}} = \frac{(4P' - \pi M)(M - 1)\sqrt{-\frac{2M^2 - 2M + 1}{M(4P' - \pi M)}}}{2\sqrt{\pi}(2M^2 - 2M + 1)} \\ D_{2,\text{opt}} + D_{1,\text{opt}} = 0.5, D_{3,\text{opt}} = 0.5, D_{4,\text{opt}} = 0 \\ D_{5,\text{opt}} = \frac{1}{4} - \frac{\sqrt{-\frac{2M^2 - 2M + 1}{M(4P' - \pi M)}} \left(\begin{array}{c} 4P' + 2\pi M^2 \\ -8MP' - \pi M \end{array} \right)}{4\sqrt{\pi}(2M^2 - 2M + 1)}. \end{cases} \quad (14)$$

The boundary line between the low-power segment and the high power-segment is $P'_b = M^2(M - 1)$. In this article, this modulation method is defined as the GMPP modulation scheme. Next, we will compare the performance of the GMPP and some

TABLE III
PARAMETERS OF THE DAB CONVERTER

Items	Descriptions	Specifications
V_I	Input Voltage	400V
V_2	Output Voltage	100V-200V
f_s	Switching Frequency	50kHz
L	Auxiliary Inductor	190μH
N	Turn Ratio	2:1

Fig. 9. rms current of various modulation schemes for (a) $M = 0.5$. (b) $M = 0.625$. (c) $M = 0.75$. (d) $M = 0.875$.

other typical modulation schemes, such as FDM and GOM, mainly including inductor rms current and ZVS operation to evaluate the effectiveness of GMPP in terms of improving efficiency.

C. rms Current Comparison

The circuit parameters of the DAB converter for comparison are summarized in Table III. To make the results more convincing, four different output voltage conditions of $V_2 = 100$ V, $V_2 = 125$ V, $V_2 = 150$ V, and $V_2 = 175$ V are selected for comparison, and the corresponding voltage conversion ratios are $M = 0.5$, $M = 0.625$, $M = 0.75$, and $M = 0.875$, respectively. The comparison results are shown in Fig. 9.

It can be seen from Fig. 9 that the inductor rms current of GMPP is greatly improved when compared with FDM and PSM, which is basically the same as GOM, regardless of voltage conversion ratio and transmission power. Therefore, from the

TABLE IV
CURRENT DIRECTION OF EACH SWITCH

primary switches				secondary switches			
S ₁	S ₂	S ₃	S ₄	Q ₁	Q ₂	Q ₃	Q ₄
i _L <0	i _L >0	i _L >0	i _L <0	i _L >0	i _L <0	i _L <0	i _L >0

perspective of rms current, GOM and GMPP have the best performance. Next, the soft-switching operation range will be compared in detail among these modulation schemes.

D. Soft-Switching Operation Range Comparison

The soft-switching operation region is another crucial indicator of converter efficiency. In recent years, with the development of new wide-band gap devices, the switching frequency of converters has been pushing toward megahertz, and the proportion of switching loss in the total losses has also increased. Moreover, if the switch operates in the hard-switching condition, a significant EMI problem may occur due to the high di/dt and dv/dt [30]. Therefore, it is important to achieve ZVS operation. Neglecting the coupling of the ac link resistance and the variable winding of the transformer, and assuming the dead time is higher than the ZVS transition time, there are at least two conditions that need to be met for the complete ZVS operation of a switch.

- 1) Current direction: before the switch is turned ON, the inductor current needs to flow through its body diode, which is the precondition to realize the ZVS. The current directions required for each switch to realize ZVS operation are shown in Table IV.
- 2) Energy storage value: the energy stored in the inductor at this time should be greater than the total energy stored in the output capacitor C_{oss} of the upper and lower arm switches [20], which can be expressed as follows:

$$Li_L^2 > 2C_{oss}V_{bus}^2 \quad (15)$$

where C_{oss} is the output capacitor of the switch and V_{bus} is the drain-source voltage during the turn-OFF period.

It is worth to mention that when the current direction of the switch is satisfied, while the energy is not enough to release the energy of the output capacitor, the switch may realize the incomplete zero-voltage switching (iZVS) [14]. This case can also reduce part of the turn-ON loss, and its value depends on the current value and the dead time. Here, $C_{oss} = 100 \text{ pF}$ based on the datasheet of the selected switch and some specific parameters are shown in Table II. Accordingly, the soft-switching range comparison results for different modulation schemes over the whole power range are shown in Fig. 10.

In Fig. 10, the purple area means that the switch operates under hard-switching condition, the yellow area means that the switch achieves iZVS, and the blank area means that the switch can achieve complete ZVS. It is noticeable that those switches that can realize ZVS over the whole power range are not included in Fig. 10. It is shown that all the switches on the secondary side of the PSM scheme cannot achieve ZVS at low and medium load. FDM has only two switches that cannot

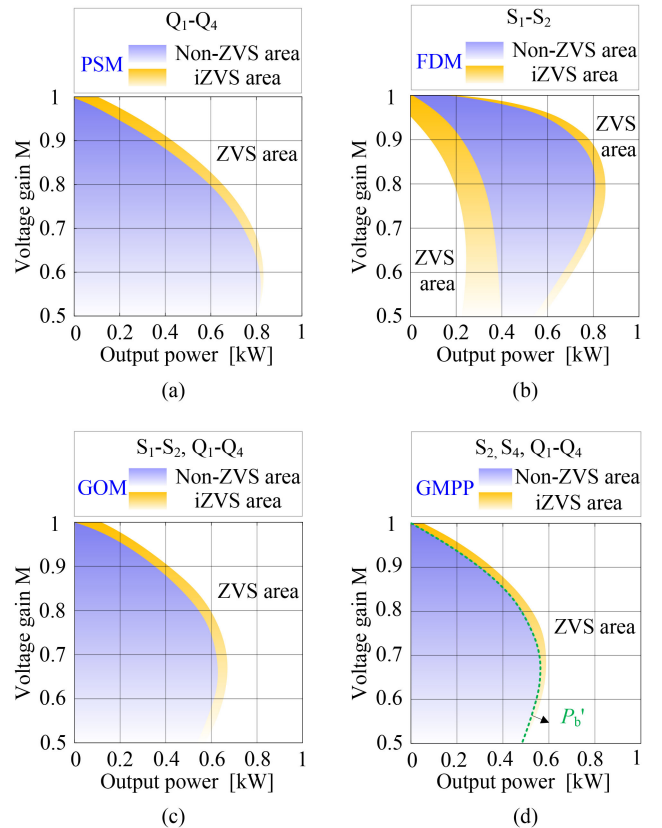


Fig. 10. ZVS performance for different modulation schemes. (a) PSM. (b) FDM. (c) GOM. (d) GMPP.

operate under soft-switching condition, while GOM and GMPP have six switches that cannot achieve soft-switching. Specially, GMPP has slight wider soft-switching operation range than GOM, but the improvement is limited. It is clear that FDM has the best soft-switching performance. Moreover, it can be seen from Fig. 10(d) that y_1 is not only the boundary line of low and high power optimization solutions but also the boundary line between iZVS and ZVS. That is to say, almost all switches in the high-power range have the possibility of realizing soft-switching. Therefore, it is necessary to expand the ZVS range of GMPP in the low-power range. In addition, it can be seen from the above analysis that it is a challenge to balance the conduction loss and switching loss with only one target. Therefore, the next section is dedicated to further expand the soft-switching range of the low-power section by adopting multi objective optimization scheme.

V. IMPROVING THE SOFT-SWITCHING RANGE OF LOW-POWER SECTION

From the analysis in Section IV, it can be seen that the GMPP can make the converter operate at the minimum current through simple optimization of the inductor peak-to-peak current. However, there are still six switches that cannot realize soft-switching under low load conditions, which degrades the efficiency of DAB converter. In order to further expand the soft-switching range, the conditions of achieving ZVS are added into the optimization

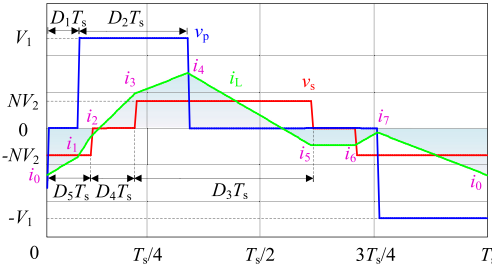


Fig. 11. General waveforms of v_p , v_s and i_L for DAB converter under mode B.

TABLE V
CURRENT CORRESPONDING TO EACH SWITCH

S ₁	S ₂	S ₃	S ₄	Q ₁	Q ₂	Q ₃	Q ₄
i_0	i_7	i_4	i_1	i_2	i_6	i_5	i_3

equation in this section. Thus, an improved optimization method is formed to reduce the peak-to-peak current and expand the soft-switching operation region.

A. Mode Analysis

Based on the above analysis, among these 11 effective modes, mode E can only transmit negative power, and modes G–J have a larger peak-to-peak current than other modes, so these modes are not analyzed. Then, from the calculation result of the optimal inductor peak-to-peak current, it can be seen that the minimum values of the modes A–D and the modes J–K are equal under nonheavy load condition, and these modes may make the converter operating with the minimum current. However, these modes show different characteristics in terms of realizing soft-switching. For mode A, as shown in Fig. 5(a), it can be seen that the ZVS conditions of switches S₂ and Q₃ are contradictory because it is required that the currents of S₂ and Q₃ are equal, but the current for switch S₂ to realize soft-switching needs to be higher than zero, and the current for Q₃ needs to be less than zero. Similarly, in mode C, the ZVS conditions of S₄ and Q₁, S₂ and Q₃ are contradictory; in mode D, the ZVS conditions of S₄ and Q₁ are contradictory; in mode J, the ZVS conditions of S₂ and Q₃ are contradictory; that is to say, no matter how to optimize these modes, there are always switches that cannot realize soft switching. Therefore, only modes B and K have the potential to ensure the minimum current and achieve soft switching for all switches simultaneously, which are discussed and analyzed below.

The typical operation waveforms of mode B are shown in Fig. 11, and the current at the switching moment of each switch is summarized in Table V. The energy required for soft-switching of primary- and secondary-side switches is different, and it can be obtained by transforming (15) to the following:

$$\begin{cases} I_{p_min} = \sqrt{\frac{2C_{oss_1}V_1^2}{L}} \\ I_{s_min} = \sqrt{\frac{2C_{oss_2}V_2^2}{L}} \end{cases} \quad (16)$$

where C_{oss_1} and C_{oss_2} are the output capacitor of the primary- and the secondary-side switches, respectively. I_{p_min} and I_{s_min} are the calculated minimum current to ensure ZVS for the primary- and the secondary-side MOSFETs.

In order to normalize the operating current, the reference value $V_1/(f_s L)$ is selected here. From (16), the following can be deduced:

$$\begin{cases} I'_{p_min} = f_s \cdot \sqrt{2C_{oss_1}L} \\ I'_{s_min} = \frac{f_s \cdot M}{N} \sqrt{2C_{oss_2}L} \end{cases} . \quad (17)$$

It can be seen from (15) that the magnitude of I'_{p_min} and I'_{s_min} is related to switching frequency f_s , inductor L , parasitic capacitance C_{oss} , and other factors. It can be seen from (3) that since the inductor current contains the square of a certain degree-of-freedom and some degrees-of-freedom are coupled with each other, it is difficult to get the analytical solution to meet the energy requirement of each switch. Fortunately, each expression contains the same complex factors, as shown in the following:

$$\zeta = \frac{D_1^2 V_1 + D_1 D_2 V_1 - D_3^2 N V_2 - D_3 D_4 N V_2}{f_s L} . \quad (18)$$

Therefore, the difference between the inductor currents at different operating moments can eliminate ζ and maintain the simplicity of the expression. Since it is unknown for all the switches to achieve soft-switching, the specific situation of each switch needs to be discussed. On the primary side, it can be seen from Fig. 11 that the maximum value of the inductor current is i_4 and the minimum value is i_0 . Therefore, switches S₁ and S₃ have the ability to realize soft-switching. Also, in order to make switches S₂ and S₄ have soft-switching capability, we can add the following restriction

$$i'_{71} = i'_7 - i'_1 > 2I'_{p_min} \quad (19)$$

where i'_7 and i'_1 represent the unit values of i_7 and i_1 , respectively. Under the constraint of inequality (19), at least one switch of S₂ and S₄ can realize ZVS turn ON. Therefore, at least three switches on the primary side can realize soft-switching. Following a similar procedure, on the secondary side, it can be seen from Fig. 11 that $i_5 = i_6$ and $i_3 > i_2$. That is to say, Q₂ and Q₃ have relevant turn-ON characteristics, and Q₄ is easier to meet ZVS conditions than Q₁. Therefore, the turn-ON current of Q₃ and Q₄ can be limited as follows:

$$i'_{25} = i'_2 - i'_5 > 2I'_{s_min} . \quad (20)$$

With the help of inequality (20), when Q₁ meets the ZVS condition, Q₄ must be able to achieve soft-switching; when Q₃ can achieve soft-switching, Q₄ must also be able to achieve it. So far, the secondary side can ensure that at least two switches can realize ZVS completely. Besides, combining inequalities (19) and (20), the ZVS operation for switch S₂ and Q₃ are uncertain, other constraints can be added to increase the possibility further, as shown in inequality (21). Although this constraint does not wholly guarantee that S₂ and Q₃ can meet the ZVS condition, it can further ensure that the current does not deviate excessively

$$i'_{75} = i'_7 - i'_5 > I'_{p_min} + I'_{s_min} . \quad (21)$$

TABLE VI
OPTIMIZED SOLUTIONS FOR MODES B AND K

	Power range	$\left[0, \frac{\pi(1-M)(2I'_{s_min} + 2MI'_{p_min} - M)^2}{2} - 2\pi I'^2_{p_min} \right]$	$\left[\frac{\pi(1-M)(2I'_{s_min} + 2MI'_{p_min} - M)^2}{2} - 2\pi I'^2_{p_min}, \frac{\pi(1-M)(M + 2I'_{p_min} - 2I'_{p_min}M)^2}{2} - 2\pi I'^2_{p_min} \right]$
mode B	Optimal solution	$D_{1,\text{opt}} = I'_{p_min} - \frac{\sqrt{(2\pi I'^2_{p_min} + P')(1-M)}}{\sqrt{2\pi}(M-1)}$ $D_{2,\text{opt}} = \frac{\sqrt{(2\pi I'^2_{p_min} + P')(1-M)} - \sqrt{2\pi}I'_{p_min}(1+M)}{\sqrt{2\pi}M}$ $D_{3,\text{opt}} = D_{1,\text{opt}} + D_{5,\text{opt}} + \frac{I'_{p_min} + I'_{s_min}}{M}$ $D_{4,\text{opt}} = 0, D_{5,\text{opt}} - D_{2,\text{opt}} = I'_{p_min}$	$D_{1,\text{opt}} = I'_{p_min} - \frac{\sqrt{(2\pi I'^2_{p_min} + P')(1-M)}}{\sqrt{2\pi}(M-1)}$ $D_{2,\text{opt}} = \frac{\sqrt{(2\pi I'^2_{p_min} + P')(1-M)} - \sqrt{2\pi}I'_{p_min}(1+M)}{\sqrt{2\pi}M}$ $D_{1,\text{opt}} + D_{5,\text{opt}} + \frac{I'_{p_min} + I'_{s_min}}{M} = 0.5$ $D_{4,\text{opt}} = 0, D_{5,\text{opt}} - D_{2,\text{opt}} = I'_{p_min}$
	Power range	$\left[0, \frac{\pi[M(1-M) - 2(I'_{p_min} + 2I'_{s_min} - 2MI'_{s_min})]^2 - 4\pi I'^2_{p_min}}{2(1-M)} \right]$	$\left[\frac{\pi[M(1-M) - 2(I'_{p_min} + 2I'_{s_min} - 2MI'_{s_min})]^2 - 4\pi I'^2_{p_min}}{2(1-M)}, \frac{\pi(2I'_{s_min} - M + M^2 + 2MI'_{p_min} - 2MI'_{s_min})^2}{2(M-1)} \right]$
mode K	Optimal solution	$D_{1,\text{opt}} = -I'_{p_min}(M-1) - \frac{\sqrt{2\pi I'^2_{p_min} + P' - MP'}}{\sqrt{2\pi}(M-1)}$ $D_{2,\text{opt}} = \frac{I'_{p_min} + 2I'_{s_min}}{M} + \frac{\sqrt{2\pi I'^2_{p_min} + P' - MP'}}{\sqrt{2\pi}M}$ $D_{3,\text{opt}} = \frac{\sqrt{2\pi}(I'_{p_min} + 2I'_{s_min} - 2MI'_{s_min}) + \sqrt{2\pi I'^2_{p_min} + P' - MP'}}{\sqrt{2\pi}M(1-M)}$ $D_{4,\text{opt}} = 0, D_{5,\text{opt}} = \frac{I'_{s_min}}{M} + \frac{\sqrt{2\pi I'^2_{p_min} + P' - MP'}}{\sqrt{2\pi}M}$	$D_{1,\text{opt}} = -I'_{p_min}(M-1) - \frac{\sqrt{2} \cdot \sqrt{2\pi I'^2_{p_min} + P' - MP'}}{2\sqrt{\pi}(M-1)}$ $D_{2,\text{opt}} = \frac{I'_{p_min} + 2I'_{s_min}}{M} + \frac{\sqrt{2} \cdot \sqrt{2\pi I'^2_{p_min} + P' - MP'}}{2M\sqrt{\pi}}$ $D_{3,\text{opt}} = 0.5, D_{4,\text{opt}} = 0$ $D_{5,\text{opt}} = \frac{I'_{s_min}}{M} + \frac{\sqrt{2} \cdot \sqrt{2\pi I'^2_{p_min} + P' - MP'}}{2M\sqrt{\pi}}$

Similarly, there are other inequality constraints

$$i'_{21} = i'_2 - i'_1 > I'_{p_min} + I'_{s_min}. \quad (22)$$

Therefore, formulas (19)–(22) can ensure more switches to realize soft-switching. These conditions are introduced into (9) to form a multiobjective optimization based on the inductor peak-to-peak current and the soft-switching range, that is, to find the minimum inductor peak-to-peak current when the soft-switching condition is satisfied. As a result, the optimized solution is shown in Table VI. The optimization ideas for mode K are similar, and the results are also shown in Table VI. The following is a comparison between the proposed multiobjective optimization solution and GMPP, from the rms current and soft switching level.

B. RMS Current Comparison

It can be seen from Table IV that after comprehensively considering the inductor peak-to-peak current and the soft-switching range, Modes B and K are established to obtain the optimal solution. Fig. 12 shows the comparison between these two modes and GMPP in terms of the rms current. It can be seen from Fig. 12 that the transmission range of the two modes is different.

Specifically, the transmission power range of mode B is larger than that of mode K, which is consistent with the conclusion in Section III. More importantly, the inductor rms current obtained by the two modes is basically the same as that of the GMPP, with no significant increase or decrease.

C. Soft-Switching Range Comparison

Fig. 13 shows the specific situation of the soft switching of each switch in the low-power section of the optimized solutions obtained by modes B and K. In Fig. 13(a), area I indicates that switches Q₂ and Q₃ have achieved iZVS, area II indicates that switch S₂ has achieved iZVS, and area III indicates that switches S₂, Q₁, and Q₄ have achieved iZVS. Area IV indicates that the switches Q₁ and Q₄ are turned ON with hard-switching, but it can be seen that this is a quite small area. In Fig. 13(b), area I represents switch S₄, Q₂, and Q₃ have achieved iZVS. By comparing with GMPP shown in Fig. 10(d), it can be found that the soft-switching range can be greatly improved. However, there are differences in the soft-switching areas of modes B and K. Specifically, mode B has only one or two switches in areas I and II that can only achieve iZVS, while mode K has three switches that can only realize iZVS.

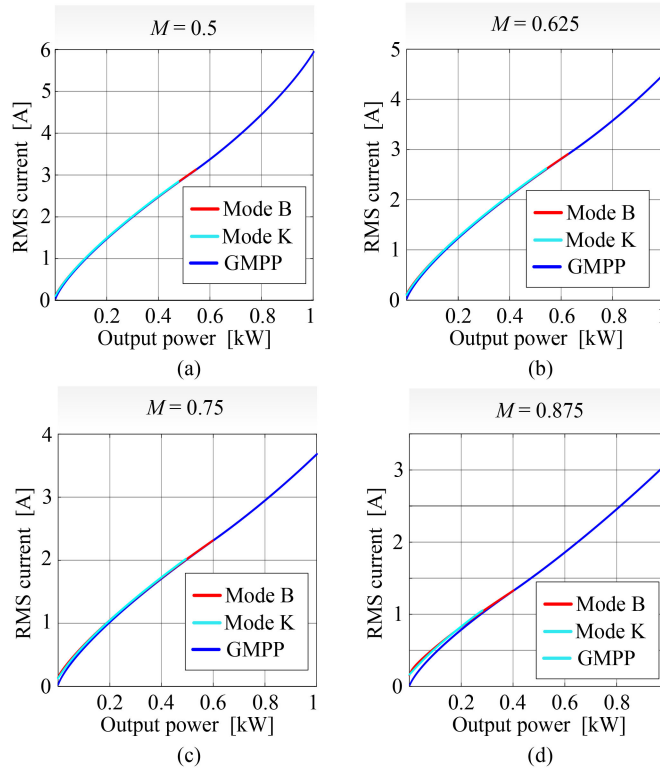


Fig. 12. RMS current comparison of mode B, mode K, and GMPP for (a) $M = 0.5$. (b) $M = 0.625$. (c) $M = 0.75$. (d) $M = 0.875$.

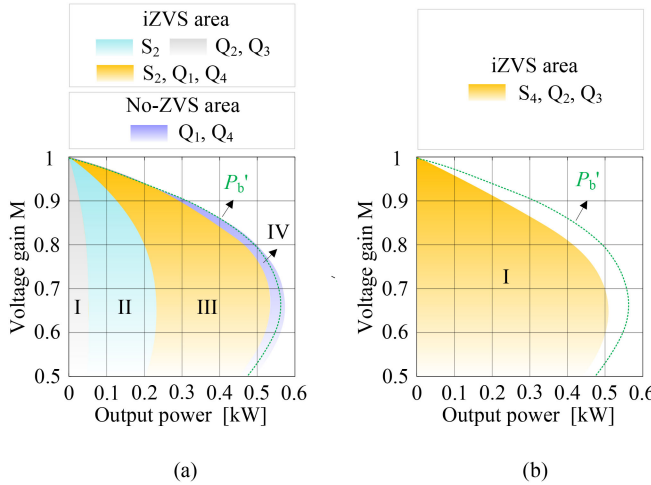


Fig. 13. ZVS performance comparison of modes B and K. (a) Mode B. (b) Mode K.

Besides, the range of the optimized solution obtained by mode B is larger than that of mode K, which is more appreciated for low-power condition. Accordingly, in the low-power range, the optimization results from mode B are eventually established.

Therefore, through the above analysis, this article finally proposes an optimized five-degree-of-freedom (O-5DOF) modulation scheme, which is divided into high- and low-power sections. Among them, the optimized solution for the low-power section is optimized by comprehensively considering the inductor peak-to-peak current and soft-switching range for mode B,

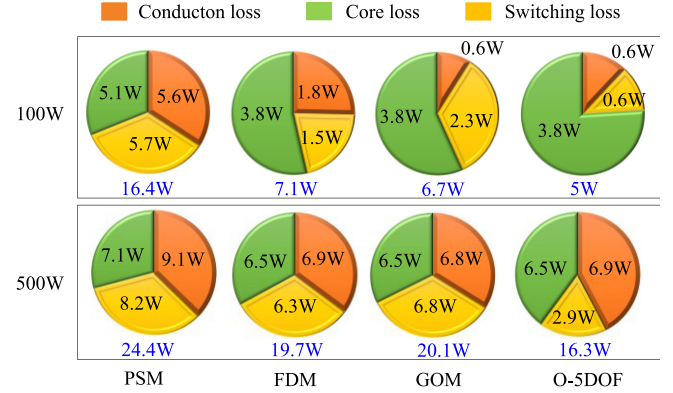


Fig. 14. Power loss analysis on various load power and voltage gain conditions for PSM, FDM, GOM, and O-5DOF schemes at $P = 100$ W and $P = 500$ W.

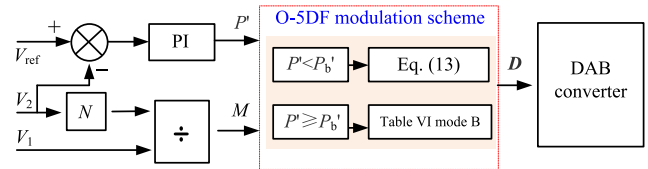


Fig. 15 Block diagram of the voltage-loop controller of the proposed O-5DOF.

while the optimized solution of the high-power section is based on GMPP. The boundary line between the low-power segment and the high-power segment is still P_b' .

Then, in order to better compare the O-5DOF with the above optimization scheme, the loss analysis results of different working conditions are given. The loss analysis of the converter is mainly composed of the following three aspects: switching losses, conduction losses, and core losses [20]. Specifically, conduction losses are calculated as the sum of $R_{DS,ON}$ conduction loss and copper loss of the magnetic components. These values are directly proportional to the square of the inductor rms current. At the same time, the influence of temperature on $R_{DS,ON}$ is simply considered here [22]. For the switching loss, a simple and effective MOSFET switching loss model is used to predict the turn-OFF and turn-ON losses under different switching currents in [22], which is based on the LTSpice simulation platform. The key to calculate the core loss is to find out the working magnetic density, which is usually related to the cross-sectional area of the magnetic device [20], and then combining with the core loss density from the material datasheet to calculate the core loss. The specific results are shown in Fig. 14.

Because the O-5DOF scheme can ensure the minimum inductor rms current, it can also maximize the soft-switching range. Therefore, it can be seen from Fig. 14 that compared to other modulation schemes, O-5DOF has smaller conduction loss and switching loss, so that O-5DOF has the highest efficiency overall. The control block diagram of [20] is used to control the steady-state algorithm proposed in this article. Its complete system control block diagram is given in Fig. 15. The output voltage V_2 is regulated by a proportional–integral controller. It is noteworthy to mention that when M is determined, P_b' is the unified value under the boundary condition, then, by comparing

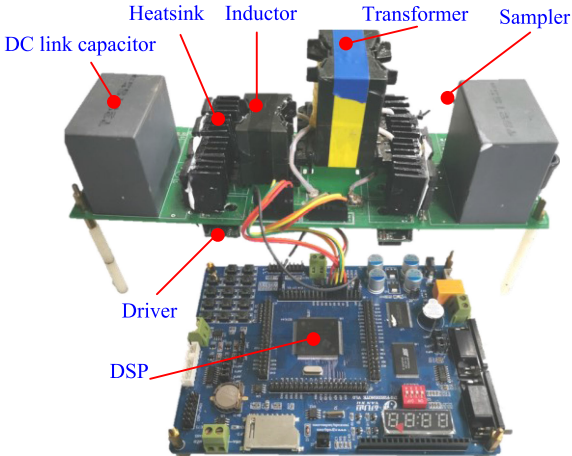
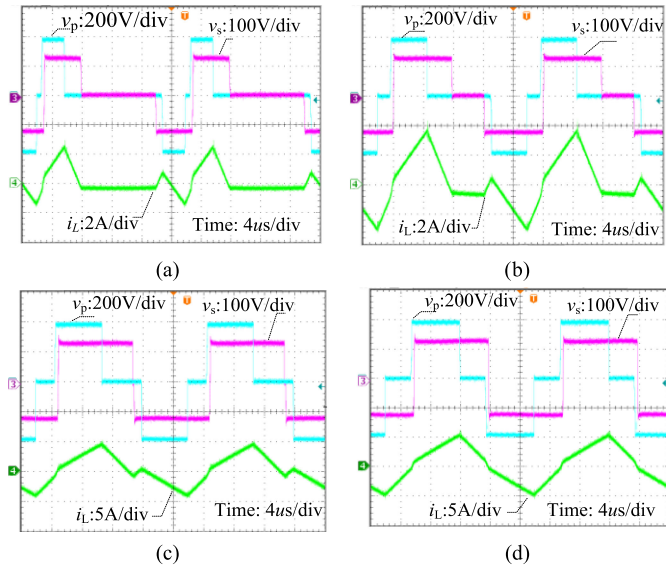


Fig. 16. Experimental prototype.

Fig. 17. Experimental waveforms of O-5DOF at $V_2 = 125$ V. (a) $P = 100$ W. (b) $P = 300$ W. (c) $P = 500$ W. (d) $P = 700$ W.

P' with P_b' , the optimal combination of \mathbf{D} can be obtained. Next, experimental results will be presented to verify the effectiveness of the optimization algorithm proposed in this article.

VI. EXPERIMENTAL RESULTS

Aiming to verify the effectiveness and correctness of the proposed O5-DOF modulation scheme for the DAB converter, a hardware prototype as shown in Fig. 16 was built. The power level and switching frequency are 1 kW and 50 kHz, respectively. Generally speaking, the dominant criterion for semiconductor selection is to achieve high efficiency, which is reflected in the ON-resistance, turn ON/OFF loss and other indicators. The silicon carbide (SiC) MOSFET SCH3060 from Rohm is selected in this article because it has the advantages of low ON-resistance, fast reverse recovery and low E_{on} and E_{off} , which leads to high efficiency performance. Finally, extensive experimental results are demonstrated in Figs. 17–21.

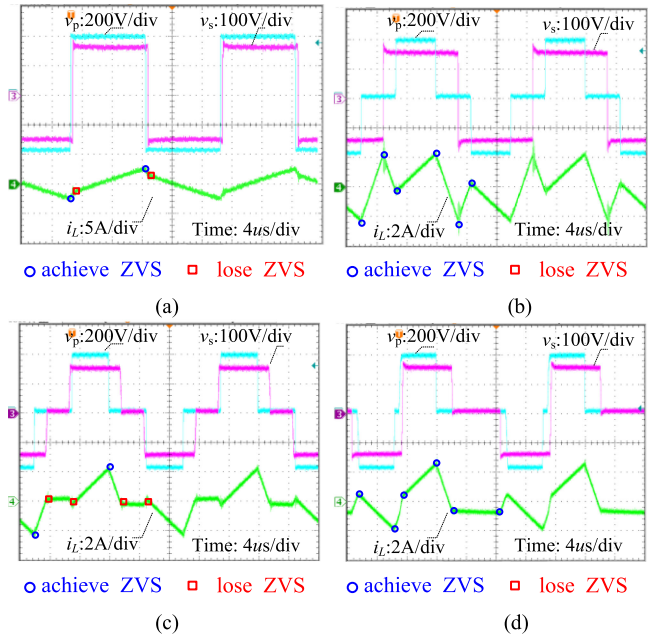
Fig. 18. Measured waveforms at different working points at $V_2 = 150$ V, $P = 200$ W. (a) PSM. (b) FDM. (c) GOM. (d) O5-DOF.

Fig. 17 shows the steady-state waveforms of the primary-side voltage v_p , secondary-side voltage v_s , and the inductor current i_L for various output power with output voltage $V_2 = 125$ V ($M = 0.625$) under the proposed O-5DOF. According to the boundary $P_b = M^2(1-M)V_1^2/(2f_sL)$ of the high- and low-power section of O-5DOF, the specific boundary value $P_b = 616$ W can be calculated when $M = 0.625$. Therefore, $P = 100, 300$, and 500 W belong to the low-power range, as shown in Fig. 17(a), (b), and (c), respectively. In the low-power range, the remarkable feature of the HF ac voltages at the primary sides of the transformer contains two unequal zero-voltage portions within one switching period, while the secondary-side voltage waveform has only one zero-voltage portion for D_4 , which is equal to 0 at this time. As the transmission power increases, D_3 is equal to 0.5 in Fig. 17(c), resulting in the secondary-side voltage not containing the zero-voltage portion. When the transmission power $P = 700$ W, it belongs to the high-power section, and the remarkable feature of the HF ac voltage at the primary side of the transformer contains two equal zero-voltage portions within one switching period, because at this time $D_1 + D_2 = 0.5$. Therefore, the feasibility of O5-DOF is verified through the above experimental results.

In order to verify the effectiveness of the O5-DOF in reducing the rms current and expanding the soft-switching range operation, Fig. 18 shows the waveforms of PSM, GOM, FDM, and O5-DOF at $P = 200$ W and $V_2 = 150$ V. First, the measured rms currents of the four modulation schemes are 1.62, 1.2, 0.98, and 1.06 A, respectively, and their theoretical values are 1.60, 1.22, 1.01, and 1.07 A, respectively. Therefore, it can be seen that the theoretical values agree with the experimental values. Table VII shows the comparison of different modulation schemes under a different transmission power and voltage conversion ratio. Through these experiments, it can be concluded that the theoretical values and the experimental values match well.

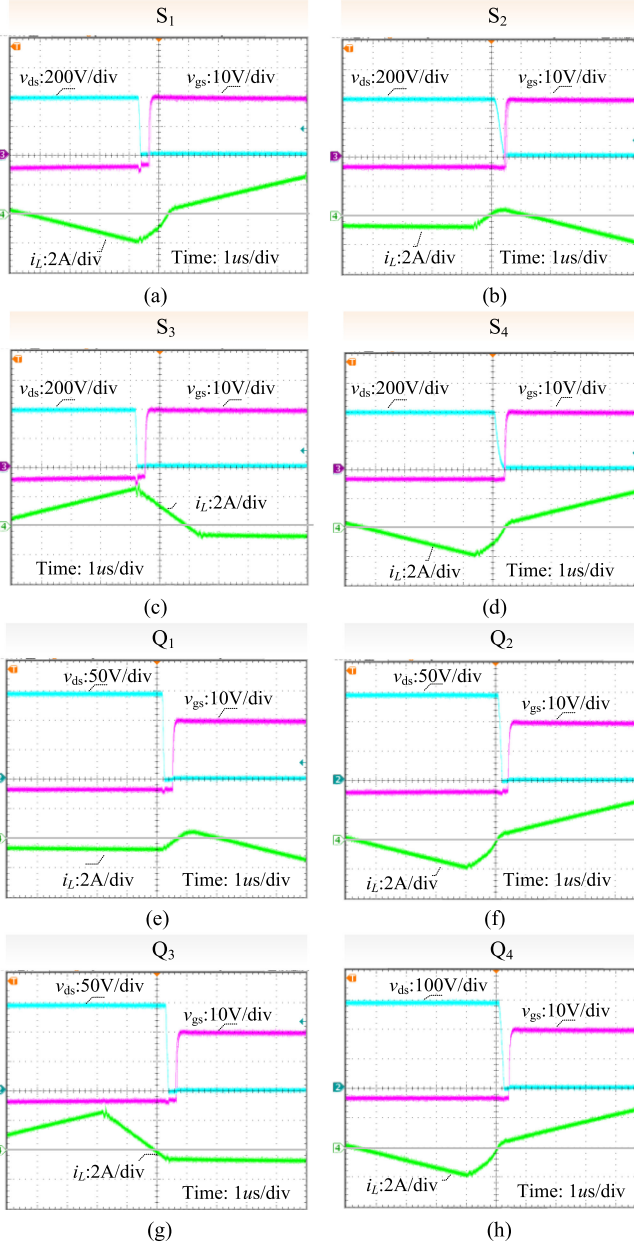


Fig. 19. Switching on of each switch under the O-5DOF at $V_2 = 150$ V, $P = 200$ W.

TABLE VII
COMPARISONS OF RMS VALUES UNDER DIFFERENT MODULATION SCHEMES

	RMS value (A)							
	PSM		FDM		GOM		O5-DOF	
	R-v	T-v	R-v	T-v	R-v	T-v	R-v	T-v
$V_2=100$ V, $P=100$ W	2.97	3.03	1.13	1.18	0.87	0.88	0.91	0.92
$V_2=100$ V, $P=500$ W	3.52	3.53	2.88	2.92	2.86	2.92	2.88	2.92
$V_2=125$ V, $P=300$ W	2.42	2.44	1.73	1.73	1.64	1.66	1.65	1.68
$V_2=150$ V, $P=600$ W	2.32	2.3	2.34	2.36	2.23	2.30	2.23	2.30
$V_2=175$ V, $P=200$ W	0.92	0.90	0.92	0.95	0.8	0.79	0.88	0.86

Note: T-v represents the theoretical value, R-v represents the actual value.

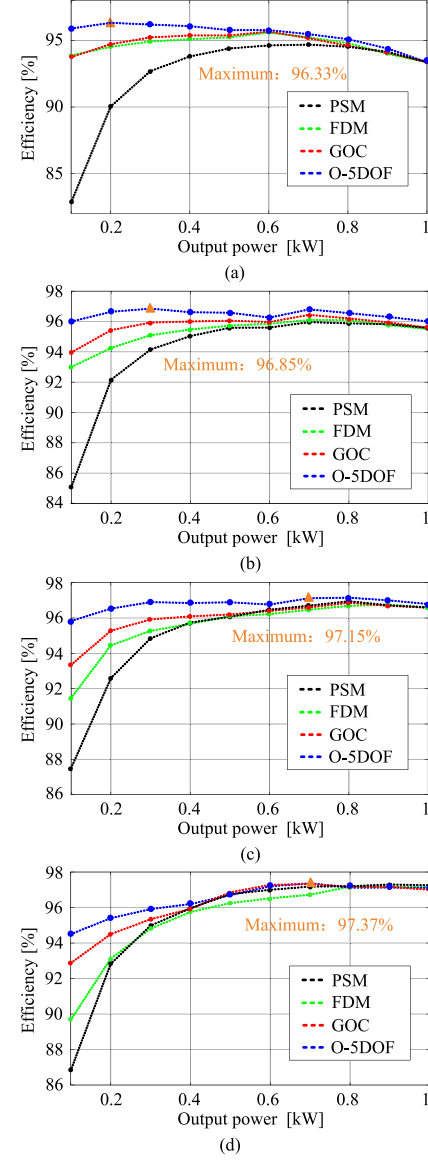


Fig. 20. Experimental efficiency curves of PSM, FDM, GOM, and O-5DOF when voltage conversion ratio M is (a) 0.5. (b) 0.625. (c) 0.75. (d) 0.875.

Next, as can be seen from Fig. 18 that different modulation schemes also have certain differences in achieving soft-switching. For the PSM scheme, as shown in Fig. 18(a), the primary and secondary sides of the transformer are square waves, and there is only one phase-shift angle between the primary and secondary sides. Therefore, the soft-switching condition for each switch on the primary side is consistent, which is similar for the secondary side. It can be seen that soft-switching is realized for the switches on the primary side of the converter, but not for the switches on the secondary side. For the FDM scheme, as shown in Fig. 18(b), all switches realize soft-switching very well. For the GOM, as shown in Fig. 18(c), when the switches S_2-S_3 and Q_1-Q_4 are turned ON, the current is basically zero, so it is difficult for these switches to achieve complete soft switching. Fig. 18(d) shows the waveforms of O5-DOF that all eight switches meet the necessary conditions for soft-switching

TABLE VIII
COMPARISON OF DIFFERENT MODULATION SCHEMES

Optimization scheme	The analysis of the optimization scheme				The result of the optimization scheme			
	Number of DOF	Combination Form	Analysis Method	Optimization objectives	Modulation Form	RMS level	soft switching range	Efficiency
Global optimal modulation (GOM) [19]	3	TPS	TDA	RMS	On-line computation	Small	Narrow	Medium
Fundamental duty modulation (FDM) [20]	3	TPS	FDA	RMS	On-line computation	Medium	Wide	Medium
Hybrid duty modulation (HDM) [23]	3	TPS +ADM	FDA	RMS	On-line computation	Medium	Wide	Medium
Optimal phase shift modulation (OPSM) [24]	3	TPS	TDA	Current stress	On-line computation	Small	Narrow	Medium
Optimal asymmetric duty modulation (OADM) [25]	3	ADM	TDA	Peak-to-peak Current	On-line computation	Small	Narrow	Medium
Particle swarm optimization (PSO) [26]	3	TPS	FDA	RMS	Off look-up table	Small	Narrow	Medium
This work	5	5-DOF	TDA	Peak-to-peak Current +ZVS	On-line computation	Small	Wide	High

from the current direction. Fig. 19 shows the detail operating waveforms associated with the eight switches, and it can be seen that all switches have realized soft switching. In the theoretical analysis, the three switches S_2 , Q_1 , Q_4 are iZVS, but they are all realized complete ZVS in practice. The main reasons are as follows.

- 1) The minimum normalized current derived from (16) itself is inaccurate. Factors such as the nonlinearity of the parasitic capacitance of the switches and the parasitic of the PCB will affect it.
- 2) The influence of dead time. Within a reasonable deadtime range [14], increasing the dead time will make some iZVS operation turn into complete ZVS.

Fig. 20 gives a comparison of the efficiency of the four modulation schemes from $M = 0.5$ to $M = 0.875$. In the test, a point is selected every 100 W for different M and P . In this way, a total of 160 points were tested, and the number of samples is large. As can be seen from Fig. 20 that the modulation scheme proposed in this article has obvious advantages in efficiency, especially under a light load. Besides, from the perspective of total loss, the theoretical calculation results are in good agreement with the experimental results under different modulation schemes and power conditions.

Dynamic performance is also an important aspect to evaluate the DAB converter under different modulation schemes. Fig. 21(a) shows the dynamic switching waveforms when the load power changes between 200 and 700 W under closed-loop

control. It can be seen that there is no obvious current and voltage overshoot, and the response time is short. Fig. 21(b) shows the waveform change when the output closed-loop voltage changes from $V_2 = 150$ V to $V_2 = 100$ V. It can be seen that when the output voltage needs to change, a quick response can be obtained.

Furthermore, in addition to FDM and GOM, in order to highlight the advantages of the modulation scheme proposed in this article, some other optimization schemes are also compared, including the hybrid duty modulation scheme [23], optimal phase-shift modulation scheme [24], optimal asymmetric duty modulation scheme [25], and particle swarm optimization modulation scheme [26]. The comparison results are summarized in Table VI. By comparison, the advantages of the proposed O-5DOF modulation scheme can be summarized as follows: First, O-5DOF is optimized on the basis of the 5-DOF modulation scheme, which not only provides the maximum optimization space, but can also unify ADM and SDM well. Second, the optimization result of O-5DOF can be calculated online to achieve continuous optimization. Also, among the various degrees-of-freedom, there are some simple relationships, such as $D_{4,opt} = 0$, $D_{2,opt} = D_{5,opt}$, and $D_{5,opt} - D_{4,opt} = I_{p-min}$ in the low-power section and $D_{4,opt} = 0$, $D_{1,opt} + D_{2,opt} = 0.5$, and $D_{3,opt} = 0.5$ in the high-power section, which can obviously reduce the computational burden. Last but not least, the O-5DOF chooses the rms and ZVS range as the optimization goal simultaneously, which greatly reduces the rms

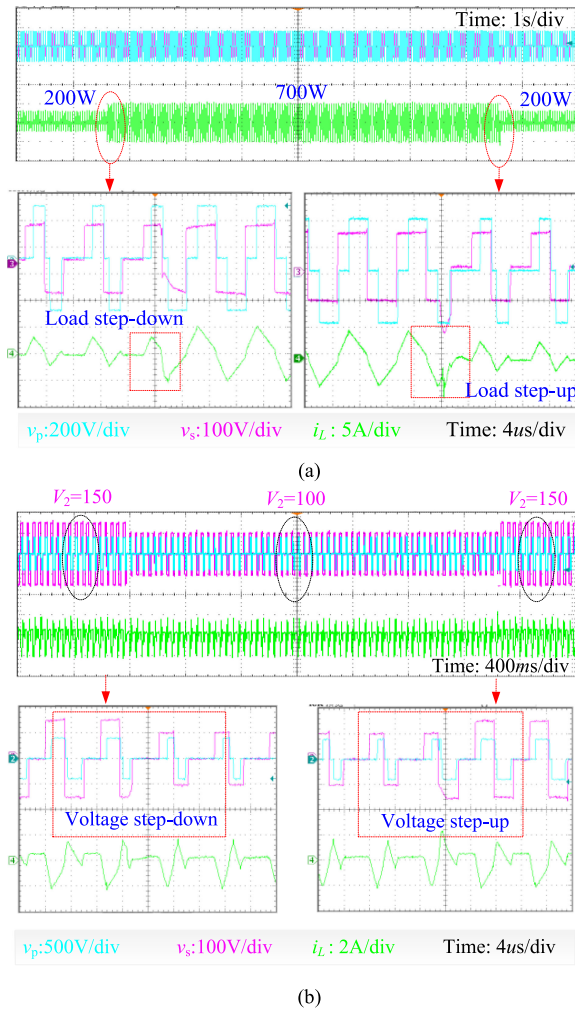


Fig. 21. Dynamic switching waveforms. (a) Load changes from 70 to 30 R. (b) Output voltage changes from $V_2 = 150$ V to $V_2 = 100$ V.

level and expands the soft-switching range to the greatest extent, and eventually improves the converter efficiency significantly, and the efficiency curve in the whole load range is smooth. The proposed O-5DOF modulation scheme can maximize the converter efficiency with acceptable computational complexity, which can be applied in real applications.

VII. CONCLUSION

In this article, the 5-DOF modulation scheme is proposed for the DAB converter. Then, the conduction loss and switching loss are both considered in the proposed O5-DOF modulation scheme to maximize the converter efficiency. The main contributions of this article are summarized as follows.

- This article first proposed a 5-DOF modulation scheme, which mainly adjusts the value and position of the zero-voltage portions in the three-level waveform by increasing the degree-of-freedom based on ADM and TPS from the perspective of the transformer terminal voltage. Therefore,

TPS and ADM are only special cases of 5-DOF modulation scheme, and the analysis of 5-DOF modulation scheme is more general.

- Based on the relative position of the primary and secondary voltages of the transformer, the mode of 5-DOF modulation scheme is discussed in detail, and their steady-state characteristics are analyzed including the inductor rms current, inductor peak-to-peak current, and transmission power, etc.
- Based on the common optimization goals of inductor peak-to-peak and soft switching range, an O-5DOF modulation scheme is proposed. O-5DOF can maximize the efficiency of the converter with acceptable computational complexity, which can be applied in real applications. This scheme basically ensures that when the inductor rms current is the smallest, all switches can achieve soft switching, thereby maximizing the efficiency of the converter.

REFERENCES

- M. Zhao, Z. zhigang, and S. Yuanyuan, "Key technologies and development prospect of new generation Low-voltage DC power supply and utilization system," China Academic Journal Electronic Publishing House, Minneapolis, MN, USA.
- X. Zhao *et al.*, "DC solid state transformer based on three-level power module for interconnecting MV and LV DC distribution systems," *IEEE Trans. Power Electron.*, vol. 36, no. 2, pp. 1563–1577, Feb. 2021.
- B. Zhao, Q. Song, W. Liu, and Y. Sun, "Overview of dual-active bridge isolated bidirectional dc–dc converter for high-frequency-link power-conversion system," *IEEE Trans. Power Electron.*, vol. 29, no. 8, pp. 4091–4106, Aug. 2014.
- Y. Xie, J. Sun, and J. S. Freudenberg, "Power flow characterization of a bidirectional galvanically isolated high-power dc–dc converter over a wide operating range," *IEEE Trans. Power Electron.*, vol. 25, no. 1, pp. 54–66, Jan. 2010.
- D. Costinett, D. Maksimovic, and R. Zane, "Design and control for high efficiency in high step-down dual active bridge converters operating at high switching frequency," *IEEE Trans. Power Electron.*, vol. 28, no. 8, pp. 3931–3940, Aug. 2013.
- F. Krämer and J. W. Kolar, "Efficiency-Optimized high-current dual active bridge converter for automotive applications," *IEEE Trans. Ind Electron.*, vol. 59, no. 7, pp. 2745–2760, Jul. 2012.
- S. Inoue and H. Akagi, "A bidirectional isolated DC–DC converter as a core circuit of the next-generation medium-voltage power conversion system," *IEEE Trans. Power Electron.*, vol. 22, no. 2, pp. 535–542, Mar. 2007.
- J. Shi, W. Gou, H. Yuan, T. Zhao, and A. Q. Huang, "Research on voltage and power balance control for cascaded modular solid-state transformer," *IEEE Trans. Power Electron.*, vol. 26, no. 4, pp. 1154–1166, Apr. 2011.
- Y. Xie, J. Sun, and J. S. Freudenberg, "Power flow characterization of a bidirectional galvanically isolated high-power DC/DC converter over a wide operating range," *IEEE Trans. Power Electron.*, vol. 25, no. 1, pp. 54–66, Jan. 2010.
- H. Bai, C. C. Mi, and S. Gargies, "The short-time-scale transient processes in high-voltage and high-power isolated bidirectional DC–DC converters," *IEEE Trans. Power Electron.*, vol. 23, no. 6, pp. 2648–2656, Nov. 2008.
- J. Hiltunen, V. Väistönen, R. Juntunen, and P. Silventoinen, "Variable-Frequency phase shift modulation of a dual active bridge converter," *IEEE Trans. Power Electron.*, vol. 30, no. 12, pp. 7138–7148, Dec. 2015.
- H. Fan and H. Li, "High-Frequency transformer isolated bidirectional DC–DC converter modules with high efficiency over wide load range for 20 kVA solid-state transformer," *IEEE Trans. Power Electron.*, vol. 26, no. 12, pp. 3599–3608, Dec. 2011.
- P. Liu and S. Duan, "A hybrid modulation strategy providing lower inductor current for the DAB converter with the aid of DC blocking capacitors," *IEEE Trans. Power Electron.*, vol. 35, no. 4, pp. 4309–4320, Apr. 2020.
- H. Shi, H. Wen, and Y. Hu, "Deadband effect and accurate ZVS boundaries of gan-Based dual-active-bridge converters with multiple-phase-shift control," *IEEE Trans. Power Electron.*, vol. 35, no. 9, pp. 9886–9903, Sep. 2020.

- [15] G. Guidi, M. Pavlovsky, A. Kawamura, T. Imakubo, and Y. Sasaki, "Efficiency optimization of high power density dual active bridge dc-dc converter," in *Proc. Int. Power Electron. Conf.*, Jun. 2010, pp. 981–986.
- [16] G. G. Oggier and M. Ordóñez, "High efficiency DAB converter using switching sequences and burst mode," *IEEE Trans. Power Electron.*, vol. 31, no. 3, pp. 2069–2082, Mar. 2016.
- [17] B. Zhao, Q. Yu, and W. Sun, "Extended-phase-shift control of isolated bidirectional dc-dc converter for power distribution in microgrid," *IEEE Trans. Power Electron.*, vol. 27, no. 11, pp. 4667–4680, Nov. 2012.
- [18] H. Bai and C. Mi, "Eliminate reactive power and increase system efficiency of isolated bidirectional dual-active-bridge dc-dc converters using novel dual-phase-shift control," *IEEE Trans. Power Electron.*, vol. 23, no. 6, pp. 2905–2914, Nov. 2008.
- [19] A. Tong, L. Hang, G. Li, X. Jiang, and S. Gao, "Modeling and analysis of a dual-active-bridge-isolated bidirectional DC/DC converter to minimize RMS current with whole operating range," *IEEE Trans. Power Electron.*, vol. 33, no. 6, pp. 5302–5316, Jun. 2018.
- [20] W. Choi, K. M. Rho, and B. H. Cho, "Fundamental duty modulation of dual-active-bridge converter for wide-range operation," *IEEE Trans. Power Electron.*, vol. 31, no. 6, pp. 4048–4064, Jun. 2016.
- [21] T. Liu *et al.*, "Design and implementation of high efficiency control scheme of dual active bridge based 10 kV/1 MW solid state transformer for PV application," *IEEE Trans. Power Electron.*, vol. 34, no. 5, pp. 4223–4238, May 2019.
- [22] R. Yu, G. K. Y. Ho, B. M. H. Pong, B. W. Ling, and J. Lam, "Computer-aided design and optimization of high-efficiency LLC series resonant converter," *IEEE Trans. Power Electron.*, vol. 27, no. 7, pp. 3243–3256, Jul. 2012.
- [23] D. Mou *et al.*, "Hybrid duty modulation for dual active bridge converter to minimize RMS current and extend soft-switching range using the frequency domain analysis," *IEEE Trans. Power Electron.*, vol. 36, no. 4, pp. 4738–4751, Apr. 2021.
- [24] S. Shao, M. Jiang, W. Ye, Y. Li, J. Zhang, and K. Sheng, "Optimal phase shift control to minimize reactive power for a dual active bridge DC-DC converter," *IEEE Trans. Power Electron.*, vol. 34, no. 10, pp. 10193–10205, Oct. 2019.
- [25] D. Mou *et al.*, "Optimal asymmetric duty modulation to minimize inductor Peak-to-Peak current for dual active bridge DC-DC converter," *IEEE Trans. Power Electron.*, vol. 36, no. 4, pp. 4572–4584, Apr. 2021.
- [26] H. Shi, H. Wen, Y. Hu, and L. Jiang, "Reactive power minimization in bidirectional DC-DC converters using a unified-phasor-based particle swarm optimization," *IEEE Trans. Power Electron.*, vol. 33, no. 12, pp. 10990–11006, Dec. 2018.
- [27] H. Shi, H. Wen, J. Chen, Y. Hu, L. Jiang, and G. Chen, "Minimum-reactive-power scheme of dual-active-bridge DC-DC converter with three-level modulated phase-shift control," *IEEE Trans. Ind. Appl.*, vol. 53, no. 6, pp. 5573–5586, Nov. 2017.
- [28] S. Hu, X. Li, and A. Bhat, "Operation of a bidirectional series-resonant converter with minimized tank current and wide ZVS range," *IEEE Trans. Power Electron.*, vol. 34, no. 1, pp. 904–915, Jan. 2019.
- [29] M. Lu, S. Hu, Y. Tang, S. Zhou, and X. Li, "A novel control strategy based on modified gating scheme for a dual-active-bridge converter," in *Proc. 12th IEEE Conf. Ind. Electron.*, 2017.
- [30] J. Chen, X. Du, Q. Luo, X. Zhang, P. Sun, and L. Zhou, "A review of switching oscillations of wide bandgap semiconductor devices," *IEEE Trans. Power Electron.*, vol. 35, no. 12, pp. 13182–13199, Dec. 2020.



Di Mou (Student Member, IEEE) was born in Lichuan, Hubei, China, in 1994. He received the B.S. degree in electrical engineering from Three Gorge University, Yichang, China, in 2017. He is currently working toward the Ph.D. degree in electrical engineering with Chongqing University, Chongqing, China.

His current research interests include bidirectional dc-dc converter, electrical vehicles, and power electronic transformers.



Quanming Luo (Member, IEEE) was born in Chongqing, China, in 1976. He received the B.S., M.S., and Ph.D. degrees in electrical engineering from Chongqing University, Chongqing, in 1999, 2002, and 2008, respectively.

He was with the Emerson Network Power Co. Ltd., Shenzhen, China, as a Research and Development Engineer from 2002 to 2005. Since 2005, he has been with the College of Electrical Engineering, Chongqing University, where he is currently a Professor. He has authored or coauthored more than

40 papers in journal or conference proceedings. His current research interests include LED driving systems, communication power systems, power harmonic suppression, and power conversion systems in electrical vehicles.



Jia Li was born in Sichuan, China, in 1996. She received the B.S. degree in electrical engineering from Southwest Petroleum University, Xining, China, in 2018. She is currently working toward the Ph.D. degree in electrical engineering with Chongqing University, Chongqing, China.

Her current research interests include bidirectional isolated dc-dc converters, control and optimization of power electronic systems.



Yuqi Wei (Student Member, IEEE) was born in Henan, China, in 1995. He received the B.S. degree from Yan'an University, Hebei, China, in 2016, and the M.S. degree from the University of Wisconsin-Milwaukee (UWM), Milwaukee, WI, USA, in 2018, and the M.S. degree from Chongqing University, Chongqing, China, in 2019, all in electrical engineering. He is currently working toward the Ph.D. degree with the University of Arkansas, Arkansas, USA.

His current research interests include topology, modeling and control of dc/dc power converters and power factor correction ac/dc converters, wide band gap devices, and active gate driving. He has published more than 30 peer-reviewed journal and conference papers.

Mr. Wei serves as a Reviewer for IEEE TRANSACTIONS ON INDUSTRIAL ELECTRONICS, IEEE TRANSACTIONS ON INDUSTRY APPLICATIONS, IEEE ACCESS, and IET Power Electronics.



Pengju Sun (Member, IEEE) received the B.S. and Ph.D. degrees in electrical engineering from Chongqing University, Chongqing, China, in 2005 and 2011, respectively.

Between September 2009 and August 2010, she was a Visiting Student with the University of California, Irvine, CA, USA. Since 2011, she has been with the College of Electrical Engineering, Chongqing University, where she is currently an Associate Professor. Her research interests include switching power converters, power quality control, and reliability of

power converter.